OLD DOMINION UNIVERSITY RESEARCH FOUNDATION

DEPARTMENT OF MECHANICAL ENGINEERING AND MECHANICS
SCHOOL OF ENGINEERING
OLD DOMINION UNIVERSITY
NORFOLK, VIRGINIA

SENSOR FOR MEASURING INSTANTANEOUS ANGLE OF ATTACK OF HELICOPTER BLADES

By

P. Stephen Barna

and

Henry W. Liu

Progress Report

Prepared for the
National Aeronautics and Space Administration
Langley Research Center
Hampton, Virginia

Under
Research Grant NSG 1143
July 1976 - July 1977
David D. Kershner, Technical Monitor
Flight Instrumentation Division

August 1977

DEPARTMENT OF MECHANICAL ENGINEERING AND MECHANICS
SCHOOL OF ENGINEERING
OLD DOMINION UNIVERSITY
NORFOLK, VIRGINIA

SENSOR FOR MEASURING INSTANTANEOUS ANGLE OF ATTACK OF HELICOPTER BLADES

By

P. Stephen Barna

and

Henry W. Liu

Progress Report

Prepared for the
National Aeronautics and Space Administration
Langley Research Center
Hampton, Virginia 23665

Under
Research Grant NSG 1143
July 1976 - July 1977
David D. Kershner, Technical Monitor
Flight Instrumentation Division

Submitted by the
Old Dominion University Research Foundation
Norfolk, Virginia 23508

August 1977

SENSOR FOR MEASURING INSTANTANEOUS ANGLE OF ATTACK OF HELICOPTER BLADES

By

P. Stephen Barna[1] and Henry W. Liu[2]

SUMMARY

During the period July 1976 to July 1977, the various research activities may be divided into three different categories:

1. improving and testing probes;
2. theoretical studies of probe motion;
3. improving research facilities.

Substantial progress was made in all aspects and it is anticipated that a satisfactory solution to the problem of measuring angle of attack of helicopter blades may be found in the near future.

SYMBOLS

b	probe constant for a real fluid flow
b_o	probe constant for ideal flow, $b_o = 2.25$
b_{12}, b_{23}	probe constants based on portholes 1, 2 and 2, 3, respectively
b_r	the ratio of b_{23} and b_{12}, $b_r = b_{23}/b_{12}$
e_{12}, e_{23}	functions that represent the dynamic effect for Δp_{12} and Δp_{23}
f	frequency, Hz

[1] Professor, Department of Mechanical Engineering and Mechanics, Old Dominion University, Norfolk, Virginia 23508.

[2] Research Assistant, Department of Mechanical Engineering and Mechanics, Old Dominion University, Norfolk, Virginia 23508.

g	gravitational acceleration, 9.81 m/sec^2
p_1, p_2, p_3	static pressures at portholes 1, 2, and 3, respectively
p_i	static pressure at point i on a sphere
p_t	total pressure
p_∞	free stream static pressure
Δp_{12}, Δp_{23}	pressure differences between portholes 1, 2 and 2,3, respectively
T	period of one complete oscillation ($T = 1/f$)
U	free stream velocity, m/sec
t	time, seconds
u, v, w	velocity components in x, y, and z directions respectively
V_i	air velocity at point i on a sphere
v_t	probe velocity under oscillating motion, m/sec
V_u , V_d	relative velocity at probe upstroke and downstroke respectively
S	stagnation point
ρ	density
θ	pitch angle, degrees
μ	viscosity
θ_D	reference displacement angle, degrees
α	half of the amplitude angle, degrees
θ_U, θ_L	pitch angle at upper and lower probe positions
ϕ	velocity potential

Subscripts

i	input
o	output
U	upper
L	lower
D	displacement

u	upstroke direction
d	downstroke direction
t	total

DESCRIPTION OF IMPROVED PROBE

The first, now outdated probe, referred to as "ODU #1," was a three-porthole spherical probe where the two transducers were arranged symmetrically as shown schematically in figure 1a. In this arrangement the pressure differences between ports 1 and 2 and 1 and 3 were measured across the transducers T_1 and T_2 respectively, where port 1 was common to both. Results of experiments performed on probe 1 were reported in Technical Report 76-T14, July 1976.

The second probe referred to as "ODU #2" is also a three-porthole spherical probe of the same dimensions as #1, where the pressure difference between ports 1 and 2 was measured with transducer T_1, while the difference between ports 2 and 3 was measured with transducer T_2, is shown schematically in figure 1b. Details of the probe are shown in figure 1c.

According to the theory of flow around a sphere, direct measurements of pressure difference $p_2 - p_3$ and $p_1 - p_2$ lead to the angle of attack, θ. In the July 1976 report, it was shown that θ can be calculated with equation (7) of that report as

$$\theta = \frac{1}{2} \tan^{-1} \left\{ \frac{1}{\frac{2(p_1 - p_2)}{(p_2 - p_3)} - 1} \right\}$$

Subsequent studies indicate, however, that the probe constant b_o, calculated on the basis of ideal fluid flow around the sphere, is somewhat different for real fluids. More particularly, the constant b_{23} for the pressure difference $p_2 - p_3$ was found to differ from the constant b_{12} related to the pressure difference $p_1 - p_2$. Theoretical considerations presented in this report show that the angle of attack can be more accurately calculated with equation 8 of Appendix A:

$$\theta = \frac{1}{2} \tan^{-1} \left\{ \frac{p_2 - p_3}{(p_2 - p_3) + 2b_r(p_1 - p_2)} \right\}$$

where the ratio $b_r = b_{23}/b_{12}$ is to be established from calibration experiments performed under steady flow conditions.

Three probes were tested during the period July 1976 to July 1977: ODU #1, ODU #2, and a probe designed by the Flight Instrumentation Division of NASA/ Langley Research Center. As indicated earlier, #2 superseded #1, while the first NASA probe proved unsatisfactory on account of the misalignment of the central port. This fault was corrected and the improved probe proved satisfactory. Only the results of probe ODU #2 are presented in this report because of space limitations.

IMPROVEMENTS TO THE TESTING EQUIPMENT

Improvements were made in two directions: (a) to produce a truly sinusoidal oscillating motion, and (b) to increase the air speed in the tunnel.

a. The first mechanism producing oscillatory motion was described in Appendix A of the July 1976 report. This mechanism was subsequently replaced in 1977 by a second mechanism called "Scotch Yoke," which is known to produce sinusoidal motion. In a "Scotch Yoke" the circular motion of a pivot is transformed into a reciprocating motion. The pivot is inserted into an elongated slot cut into a crosshead that is provided with guides. As the pivot rotates the slot translates parallel with itself. Details of the Scotch Yoke are shown in figure 2a. The mechanism was designed to fit the existing experimental apparatus.

b. Improvement to the wind tunnel was necessary because of the inefficient fan and unsatisfactory "Vee belt" drive. Access to the pulley to the drive shaft was attained through a large, 14-in. diameter, funnel, which partially obstructed the flow downstream from the fan blades. Subsequently, the fan blades were redesigned and the funnel was eliminated by changing the "Vee belt" drive to a front-end direct-drive through a floating shaft. The new fan was provided with a redesigned set of downstream guide vanes which were housed inside a new and much improved housing (fig. 2b). The process of redesigning, together

with the problems encountered in the process of manufacturing the components, plus the installation, took longer than a year and entailed a massive coordination of effort to complete. The performance of a new fan proved 100 percent satisfactory as it increased the air speed from about 65 ft/sec to 100 ft/sec, and the dynamic pressure, q, by a factor of two!

THEORETICAL STUDIES OF PROBE MOTION

The probe motion at present is still subject to theoretical studies. The oscillating motion of the sphere on a semicircular path may be considered as the result of three component motions: up and down (vertical component); back and forth (horizontal component); and turning about its horizontal axis (rotary component). Solution to the horizontal motion has been found in the literature, and a similar solution to the vertical component may be found in the near future. The rotary component will probably cause no great problem. However, the difference between theoretical (potential flow) solutions may differ from the real effects, and comparative experiments may become necessary on the component motions to verify theory.

EXPERIMENTAL RESULTS

Steady Flow Tests

Results of steady-flow tests are based on the pitch angle θ measured from the horizontal datum line. The stagnation point S shown in figure 3a is only applicable to steady flow and is located where the horizontal velocity vector U contacts the surface of the sphere. In the steady-flow test, the pitch angle was varied from the lowest, $\theta_L = -30$, to the highest (upper), $\theta_U = +30$, by steps with the probe "fixed" in space while the observations were made.

Tests on the ODU #2 probe were performed under various air speeds in the range of Reynolds numbers* 2.37 to 6.25×10^4 (corresponding to air velocities of 38 to 100 ft/sec). In figure 4 the normalized pressure difference $\Delta p_{23}/q$ and $\Delta p_{12}/q$ are plotted against pitch angle θ. More particularly in figure

---

* The Reynolds number may be calculated from the formula Re = 625 U, where U is in ft/sec.

4a both pressures are plotted against θ, while in figures 4b and 4c the same quantities are plotted against sin 2θ and $1/\sqrt{2}$ sin $(\pi/4 - 2\theta)$, respectively. It appears from figure 4b that the probe constant $b_{23} = 1.8$ to 1.9 and from figure 4c $b_{12} = 1.9$ to 2.0, the exact value depending on the Reynolds number used. The ratio $b_r = b_{23}/b_{12}$ is plotted against the Reynolds number in figure 4d.

From the results thus obtained it is possible to predict the output angle θ_{out} using equation (8) given in Appendix A. In figure 5 the output angle θ_{out} is plotted against the input angle θ_{in}, the latter being measured with a clinometer, while the former was calculated assuming $b_r = 0.857$. Some disagreement with θ_{in} is noticeable due to experimental error. The discrepancy, however, may be considered small. Variation in b_{23} and b_{12} were found to be strongly dependent on Reynolds number, especially in the subcritical range ($Re < 2 \times 10^5$); no data in the supercritical range ($Re > 2 \times 10^5$) are available at this time.

Tests With Oscillating Probe

Tests with the probe oscillating fall into the unsteady flow category because the flow pattern about the sphere changes with time. Under oscillating motion the spherical probe head follows a circular arc path enclosing an amplitude angle 2α. Measured from the datum are the central "extreme" angles θ_L and θ_U, at which the sphere velocity, $-v_t$, is zero; while at the displacement angle θ_D, the sphere moves with maximum speed. It may be seen from figure 3a that

$$2\alpha = \theta_L + \theta_U$$

and

$$\theta_D = \alpha - \theta_L = \theta_U - \alpha \quad .$$

The probes were tested in a frequency range 1 to 5 with air speed varying from 38 to 100 ft/sec. Amplitude was set at a nominal $2\alpha = 18$ degrees, while displacement, θ_D, was varied from 0 to 15 degrees.

Results of tests performed under oscillations are presented in figures 6 to 9, where the normalized pressure differences $\Delta p_{23}/q$, $\Delta p_{12}/q$ are plotted

against θ. The abscissa consists of two parts: the upstroke and the downstroke. The upstroke motion starts with $\theta = \theta_L$, shown at far left, and finishes at $\theta = \theta_U$ at center; the downstroke starts with $\theta = \theta_U$ at center and finishes with $\theta = \theta_L$ at the far right. The time for the complete period is $T = 1/f$.

The difference in the curves between the up and down stroke may be partly explained by first considering the velocity vector diagram shown in figure 3b. During the upstroke, the stream velocity U and probe velocity $-v_t$ combine into the relative velocity V_u, while during the downstroke they combine into V_d. When displacement θ_D is different from zero $V_u > V_d$ and $V_u^2 >> V_d^2$, hence the pressure differences change accordingly. In addition to the change in relative velocity the stagnation point also changes location. During the upstroke S' will be located below S (S being the steady flow stagnation), while during the downstroke S'' will be located above S.*

Further, theory indicates that under unsteady flow conditions the steady flow Bernoulli equation must be corrected by adding the term $d\phi/dt$, where ϕ is the velocity potential. Accordingly, the pressure difference between ports increases above the value calculated for steady flow conditions when $f = 0$.

The curves presented in figures 6 to 9 are results of "parametric" studies. Because of the variables U, f, 2α, θ_D, and probe geometry, it is only possible to study the effects by varying only one parameter at a time while keeping all others constant. During one set of experiments, the probe geometry, 2α, the Reynolds number of the sphere, and θ_D were kept constant leaving only f as variable. The experiments were repeated for various values of θ_D. Still, in another set of experiments f was kept constant and the Reynolds number was varied, and so on. The set of data thus obtained were plotted on each diagram for a particular Re and θ_D, where $2\alpha = 18$ degrees for all figures presented (figs. 6, 7, 8, and 9). Note that if 2α were to be replaced by the time, T, of a complete cycle of oscillations, the abscissa spreading over 2α would inversely decrease with increasing frequency ($T = 1/f$). These experiments were repeated for various Reynolds numbers.

Since the velocity of the oscillating probe is zero at each end of the "stroke" (θ_L, θ_U), the pressure difference should approximately equal the steady flow values. It appears, however, that the steady flow values are somewhat lower, which may be attributed to inertia effects in the flow. The boundary layer moving in the flow direction during an upstroke probably keeps

* Note: S' and S'' are not shown.

on moving in that direction for a short period of time even after the motion of the sphere is stopped, and may retain its motion after the sphere motion is reversed from upstroke to downstroke.

It appears from figures 6 to 9 that for the lower Reynolds numbers, the effect of frequency on the pressure difference is greater than at higher Reynolds numbers. This may be explained by considering the relative magnitude of the velocity vectors U and v_t. At higher Reynolds numbers the length of U vector increases (see fig. 3b), and the resultant relative velocity V is then largely controlled by U. It may be anticipated that under actual operating conditions, when the Mach number attains values of 0.5 at the probe location on the helicopter blade, the effect of oscillatory motion on the overall performance of the probe will become negligible. This assumption, however, needs to be confirmed by experiments on the probe with very high velocity air streams which are unavailable at present at Old Dominion University.

EFFECT OF REYNOLDS NUMBER AND FREQUENCY

Variation of Δp_{23} and Δp_{12} with frequency may be studied in figure 10. The curves shown in figure 10a are of sinusoidal character. The solid line corresponding to "zero" frequency (very slow motion) is, of course, purely sinusoidal and was established from "steady flow" results shown in figure 4. The increase of frequency to $f \approx 2$ results in a higher peak which occurs earlier, and a further increase to $f \approx 5$ shows similar effect. Since during these experiments the air velocity approaching the probe remained constant, one concludes that increase in frequency has two effects: (a) increase in pressure difference due to the unsteady flow effects; and (b) the occurrence of pressure peaks progressively earlier with increasing frequency. This is clearly an out-of-phase effect, and is partly due to the stagnation point changing its position relative to the steady flow location shown as S in figure 3. The other factor is probably due to inertia effects in the boundary layer. These effects are less marked in figure 10b.

Variation of Δp with air speed (corresponding to Reynolds number changes) (see fig. 11) shows for constant frequency a reverse trends as compared with frequency changes because the increase in air speed brings the higher air speed

curves closer to the steady flow (f = 0) case. This result is of great importance because it clearly indicates that performance of the probe under very high air speed ($M \sim 0.5$) conditions may be predicted from steady flow experiments for a known frequency.

Experiments with high speed air flow ($U \sim 300$ ft/sec) have recently been started, but no results are available at the time of writing this report.

APPENDIX A

THEORETICAL CONSIDERATIONS

STEADY FLOW

For steady uniform flow conditions of an ideal fluid passing over a perfectly spherical object, the pressure at a point i on the surface is

$$p_i = p_t - \frac{1}{2} \rho V_i^2 \tag{1}$$

where p_i and V_i are the static pressure and the relative surface velocity respectively at point i on the sphere, and p_t is the stagnation pressure.

The pressure coefficient for a spherical object may be derived from potential flow theory and is given by

$$\frac{p_i - p_\infty}{\frac{1}{2} \rho U^2} = 1 - b_o \sin^2 \theta \tag{2}$$

where θ is the central angle enclosed between point i and the stagnation point S (see fig. A1). Potential flow theory yields a sphere constant b_o equal to exactly 2.25.

For a real fluid flow, it appears convenient to employ a relation similar to equation (2),

$$\frac{p_i - p_\infty}{\frac{1}{2} \rho U^2} = 1 - b \sin^2 \theta \tag{3}$$

where the sphere constant b is expected to differ from b_o; however, its value needs to be established from experiments. Note that equation (3) usually holds only for angles of $\theta \leq 60$ degrees.

Pressure differences existing between any two points on the sphere may be established with equation (3). Consider the pressures at the side portholes 2 and 3 as shown in figure 1. Let the pressure at point 2 be

$$p_2 = p_t - b\, q \sin^2 \theta_2$$

and at point 3

$$p_3 = p_t - b\, q \sin^2 \theta_3$$

where

$$q = \frac{1}{2} \rho U^2 \quad .$$

The pressure difference $\Delta p_{23} = p_2 - p_3$ between side ports 2 and 3 is obtained by subtraction:

$$\Delta p_{23} = p_2 - p_3 = b\, q(\sin^2 \theta_3 - \sin^2 \theta_2) \tag{4}$$

Let the central angle enclosed between ports 2 and 3 be exactly 90 degrees, $\theta_2 + \theta_3 = \pi/2$ and let $\theta = (\theta_3 - \theta_2)/2$. Upon substitution one obtains

$$\Delta p_{23} = q\, b_{23} \sin 2\theta \tag{5}$$

where the value of b_{23} depends on the location of ports 2 and 3.

The pressure difference between center port 1 and side port 2 may be expressed as

$$\Delta p_{12} = p_1 - p_2 = \frac{1}{\sqrt{2}}\ b_{12} \sin\left(\frac{\pi}{4} - 2\theta\right) \tag{6}$$

where the sphere constant b_{12} depends on the location of the side port (relative to the center port).

Combination of equations (5) and (6) yields

$$\cos 2\theta = \frac{\Delta p_{23}}{b_{23} q} + \frac{2\Delta p_{12}}{b_{12} q} \tag{7}$$

Upon dividing equation (5) with (7), one obtains

$$\tan 2\theta = \frac{\Delta p_{23}}{\Delta p_{23} + 2\left(\frac{b_{23}}{b_{12}}\right)\Delta p_{12}}$$

or

$$\theta = \frac{1}{2}\tan^{-1}\left[\frac{\Delta p_{23}}{\Delta p_{23} + 2b_r\,\Delta p_{12}}\right] \tag{8}$$

where $b_r = b_{23}/b_{12}$.

UNSTEADY FLOW

Consider the X component of the Navier-Stokes equations

$$\frac{\partial u}{\partial t} + u\frac{\partial u}{\partial x} + v\frac{\partial u}{\partial y} + w\frac{\partial u}{\partial z} = -g\frac{\partial h}{\partial x} - \frac{1}{\rho}\frac{\partial p}{\partial x} + \frac{\mu}{\rho}\left(\frac{\partial^2 u}{\partial x^2} + \frac{\partial^2 u}{\partial y^2} + \frac{\partial^2 u}{\partial z^2}\right) \tag{9}$$

For irrotational flow

$$\frac{\partial w}{\partial y} = \frac{\partial v}{\partial z}\ , \qquad \frac{\partial u}{\partial z} = \frac{\partial w}{\partial x}\ , \qquad \frac{\partial v}{\partial x} = \frac{\partial u}{\partial y}$$

hence, equation (9) can be written

$$\frac{\partial u}{\partial t} + \frac{\partial}{\partial x}\left(\frac{u^2 + v^2 + w^2}{2}\right) = -g\frac{\partial h}{\partial x} - \frac{1}{\rho}\frac{\partial p}{\partial x} + \frac{\mu}{\rho}\frac{\partial}{\partial x}\left(\frac{\partial u}{\partial x} + \frac{\partial v}{\partial y} + \frac{\partial w}{\partial z}\right)$$

Since for incompressible flow

$$\frac{\partial u}{\partial x} + \frac{\partial v}{\partial y} + \frac{\partial w}{\partial z} = 0$$

one obtains

$$\frac{\partial u}{\partial t} + \frac{\partial}{\partial x}\left(\frac{V^2}{2}\right) + g\frac{\partial h}{\partial x} + \frac{1}{\rho}\frac{\partial p}{\partial x} = 0 \qquad (10a)$$

where $V^2 = u^2 + v^2 + w^2$.

Similarly for the Y and Z components one obtains

$$\frac{\partial v}{\partial t} + \frac{\partial}{\partial y}\left(\frac{V^2}{2}\right) + g\frac{\partial h}{\partial y} + \frac{1}{\rho}\frac{\partial p}{\partial y} = 0 \qquad (10b)$$

$$\frac{\partial w}{\partial t} + \frac{\partial}{\partial z}\left(\frac{V^2}{2}\right) + g\frac{\partial h}{\partial z} + \frac{1}{\rho}\frac{\partial p}{\partial z} = 0 \qquad (10c)$$

For potential flow

$$u = \frac{\partial \phi}{\partial x} \quad , \qquad v = \frac{\partial \phi}{\partial y} \quad , \qquad w = \frac{\partial \phi}{\partial z}$$

the time derivatives of the velocity components become

$$\frac{\partial u}{\partial t} = \frac{\partial^2 \phi}{\partial t \partial x} \quad , \qquad \frac{\partial v}{\partial t} = \frac{\partial^2 \phi}{\partial t \partial y} \quad , \qquad \frac{\partial w}{\partial t} = \frac{\partial^2 \phi}{\partial t \partial z}$$

Therefore equation (10) may be written

$$\frac{\partial}{\partial x}\left(\frac{\partial \phi}{\partial t}\right) + \frac{\partial}{\partial x}\left(\frac{V^2}{2} + gh + \frac{p}{\rho}\right) = 0 \qquad (11a)$$

$$\frac{\partial}{\partial y}\left(\frac{\partial \phi}{\partial t}\right) + \frac{\partial}{\partial y}\left(\frac{V^2}{2} + gh + \frac{p}{\rho}\right) = 0 \qquad (11b)$$

$$\frac{\partial}{\partial z}\frac{\partial \phi}{\partial t} + \frac{\partial}{\partial z}\left(\frac{V^2}{2} + gh + \frac{p}{\rho}\right) = 0 \qquad (11c)$$

Ignoring gravitational effects, one obtains upon integration

$$\frac{\partial \phi}{\partial t} + \frac{V^2}{2} + \frac{p}{\rho} = F(t) \qquad (12)$$

where $F(t)$ is a function of time only. Since the above relation holds for the entire field of motion at a given time $t = t_1$ we may write for ports 2 and 3

$$\left(\frac{\partial\phi}{\partial t} + \frac{V^2}{2} + \frac{p}{\rho}\right)_{\text{at point 2}} = \left(\frac{\partial\phi}{\partial t} + \frac{V^2}{2} + \frac{p}{\rho}\right)_{\text{at point 3}}$$

hence

$$\left[\frac{1}{2} V_2^2 + \frac{p_2}{\rho}\right] - \left[\frac{1}{2} V_3^2 + \frac{p_3}{\rho}\right] = \left[\left(\frac{\partial\phi}{\partial t}\right)_3 - \left(\frac{\partial\phi}{\partial t}\right)_2\right]$$

Thus, based on the equation of motion the simultaneous pressure difference between ports 2 and 3 becomes

$$\frac{p_2 - p_3}{\rho} = \frac{1}{2}(V_3^2 - V_2^2) + \left[\left(\frac{\partial\phi}{\partial t}\right)_3 - \left(\frac{\partial\phi}{\partial t}\right)_2\right]$$

or

$$\Delta p_{23} = \frac{1}{2}\rho(V_3^2 - V_2^2) + \rho\left[\left(\frac{\partial\phi}{\partial t}\right)_3 - \left(\frac{\partial\phi}{\partial t}\right)_2\right] \tag{13}$$

The first term on the right-hand side of equation (13) is independent of time, while the second term may depend on both space and time. It may well be that the first term could be replaced by equation (5), while the second term could be replaced by some function of the kinetic energy, space, and time. Thus

$$\Delta p_{23} = \frac{1}{2}\rho U^2 \, b_{23} \sin 2\theta + \frac{1}{2}\rho U^2 \cdot a(x,t) \tag{14}$$

Since the probe performs an oscillating motion, the space and time variables may be interchanged with velocity and frequency of oscillations. Introducing

$$e_{23}(U,f) = \frac{a(x,t)}{b_{23} \sin 2\theta(t)}$$

upon substitution into equation (14) one obtains

$$\Delta p_{23} = q\, b_{23}\left[1 + e_{23}(U,f)\right]\sin 2\theta(t) \tag{15}$$

where $q = \frac{1}{2}\rho U^2$. Similarly

$$\Delta p_{12} = q\, b_{12}\,\frac{1}{\sqrt{2}}\left[1 + e_{12}(U,f)\right]\sin\left(\frac{\pi}{4} - 2\theta\right) \tag{16}$$

DETERMINATION OF b_{23}, b_{12}, and $e(U,f)$

The constants b_{23} and b_{12} can be determined from experimental data obtained from wind tunnel tests. Equations (5) and (6) can be rewritten as

$$b_{23} = \frac{\Delta p_{23}}{q\ \sin 2\theta} \tag{17a}$$

and

$$b_{12} = \frac{\Delta p_{12}}{\frac{1}{\sqrt{2}}\, q\ \sin\left(\frac{\pi}{4} - 2\theta\right)} \tag{17b}$$

Since all the terms on the right-hand side of equation (17) can be measured in steady flow tests, the sphere constants b_{23} and b_{12} can be evaluated (see figures 2b and 2c).

The unsteady effect on $e(U,f)$ was expected to be strongly dependent on the oscillating frequency. The probe pitching angle $\theta(t)$ can be written as

$$\theta(t) = \theta_D + \alpha \sin(2\pi f t) \tag{18}$$

where θ_D is the reference displacement angle, α is half of the amplitude angle, and f is the oscillating frequency. By comparison of equations (5)

and (6) and (15) and (16), it appears that for the case $f = 0$, $e_{12}(U,f) = 0$, and $e_{23}(U,f) = 0$.

In order to study $e_{12}(U,f)$ and $e_{23}(U,f)$ rewrite equations (15) and (16) as

$$\frac{\Delta p_{12}}{b_{12}\, q} = \left(1 + e_{12}(U,f)\right) \cdot \frac{1}{\sqrt{2}} \sin\left(\frac{\pi}{4} - 2\theta(t)\right) \tag{19}$$

and

$$\frac{\Delta p_{23}}{b_{23}\, q} = \left(1 + e_{23}(U,f)\right) \cdot \sin\left(2\theta(t)\right) \tag{20}$$

The difference between unsteady and steady motion then can be analyzed, and the value for e_{23} and e_{12} can thus be found. These studies are still being pursued at the time of writing this report.

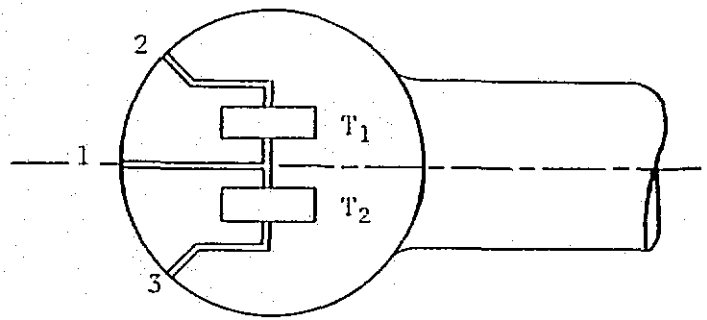

Figure 1(a). ODU probe #1.

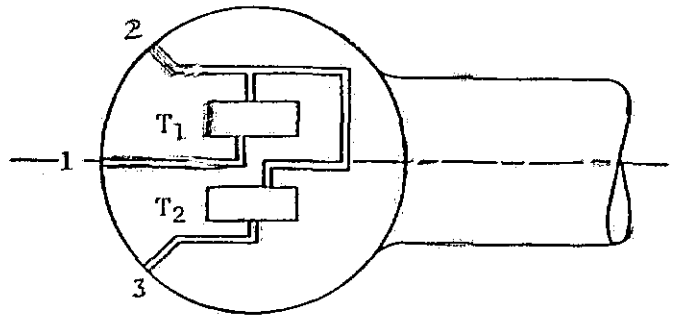

Figure 1(b). ODU probe #2.

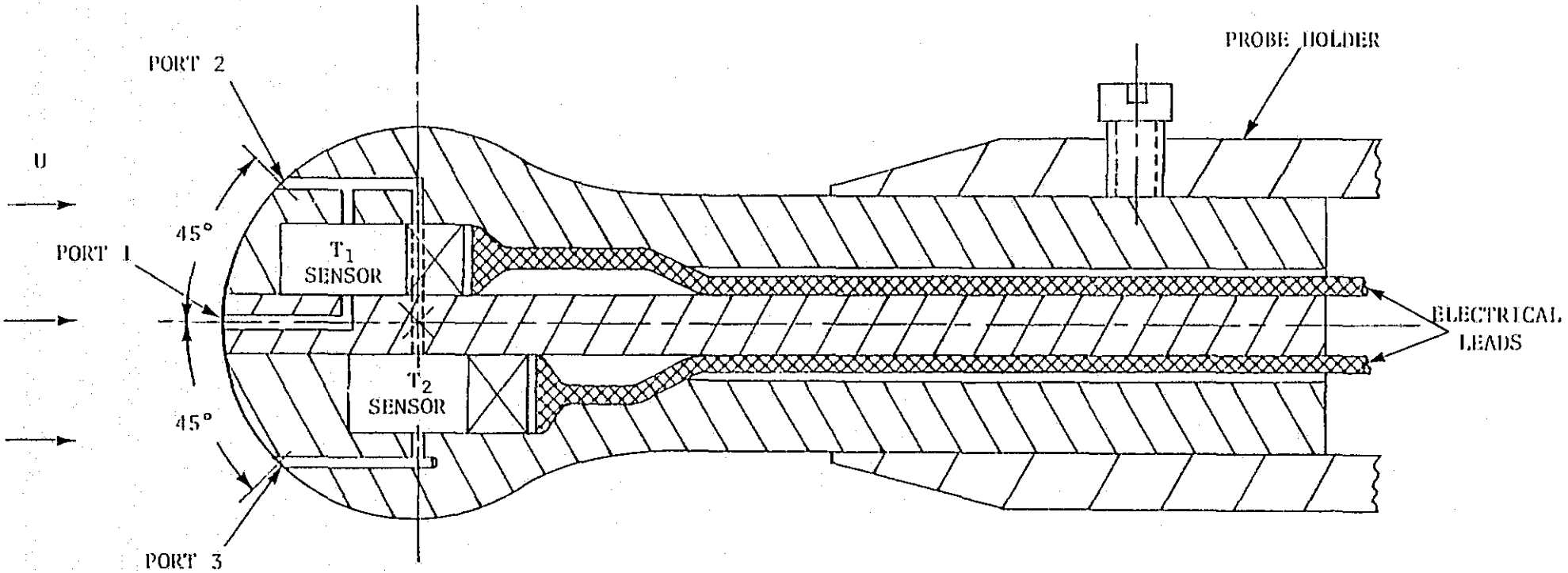

Figure 1(c). ODU #2 spherical probe showing sensors T_1 and T_2 and ports 1, 2, and 3.

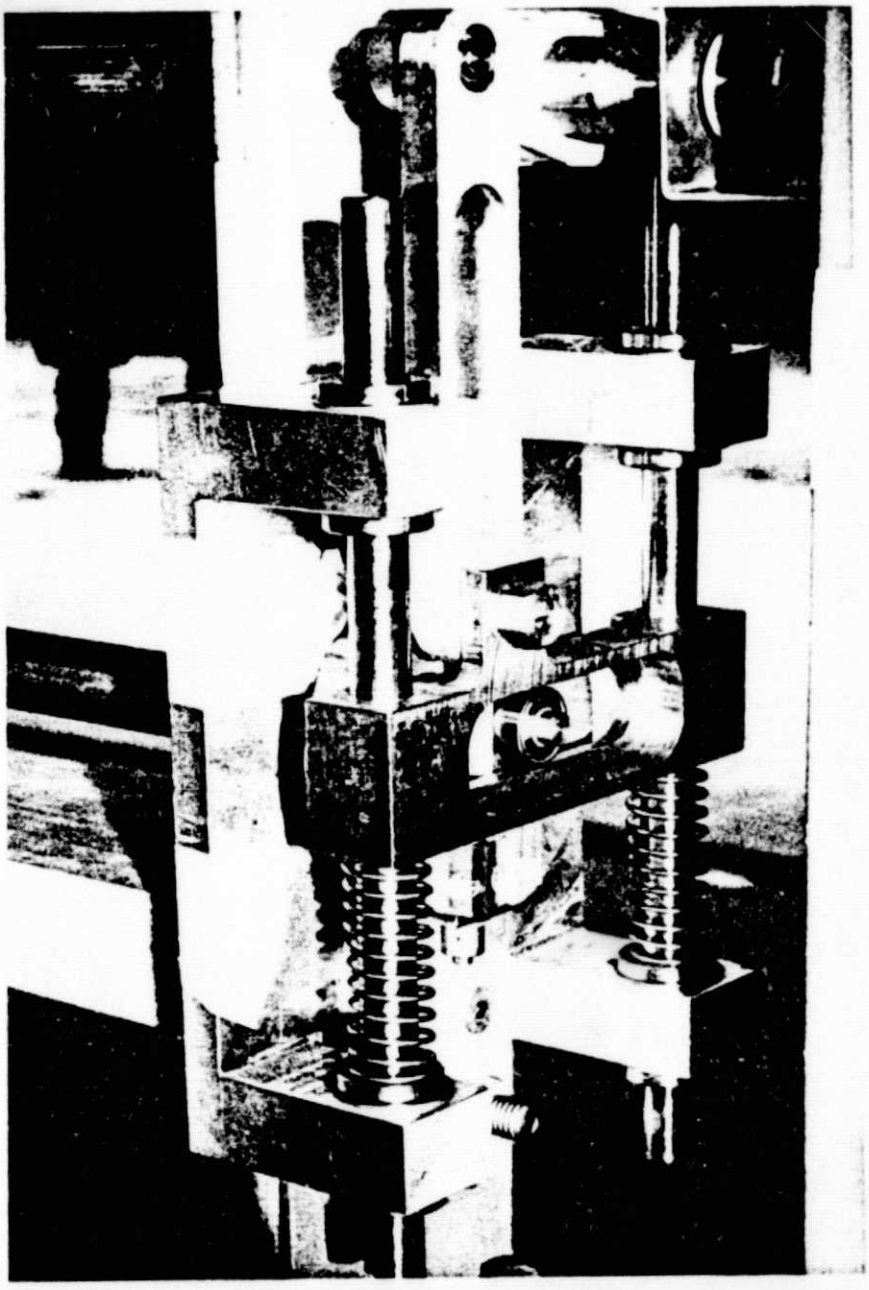

Figure 2(a). View of the Scotch yoke.

Figure 2(b). Front view of the remodeled axial flow fan.

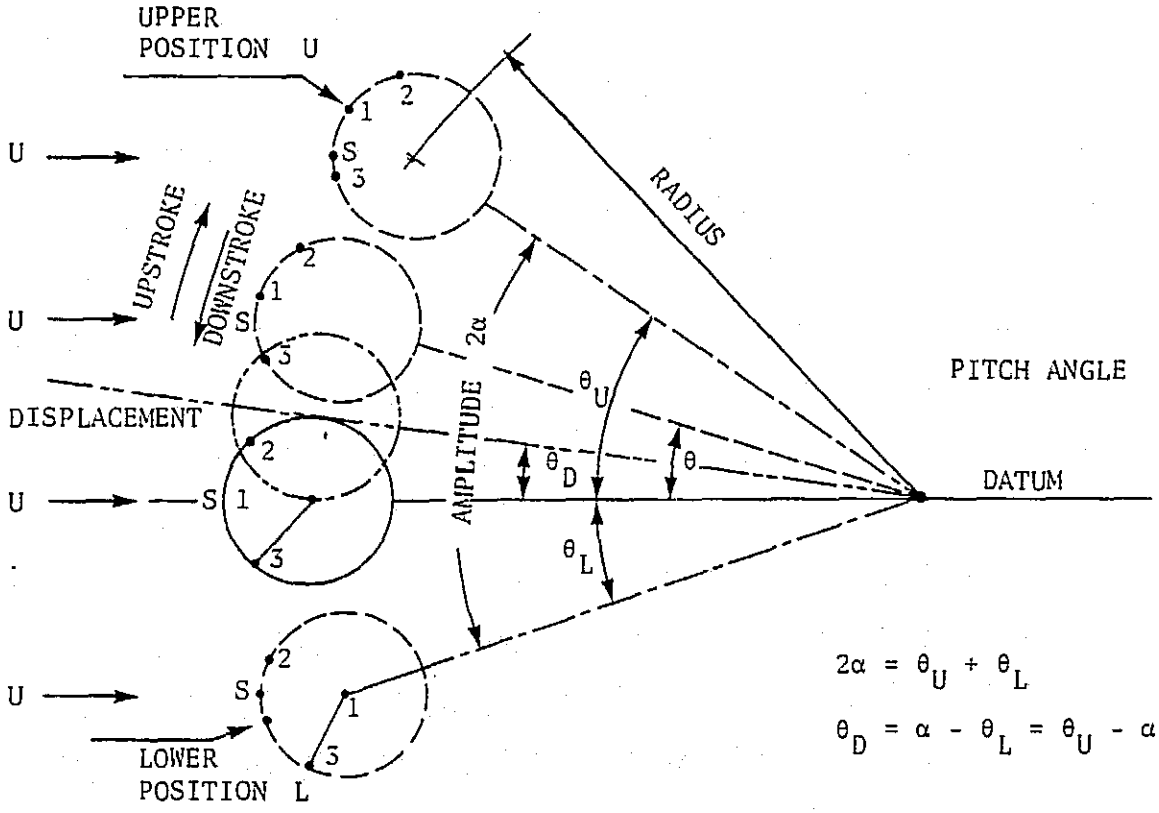

Figure 3(a). Various positions of oscillating probe.

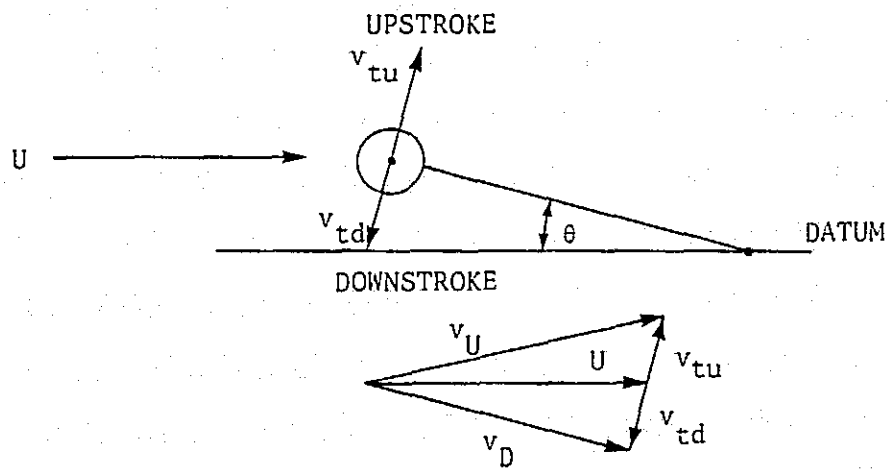

Figure 3(b). Velocity vectors during upstroke and downstroke at the same θ angle.

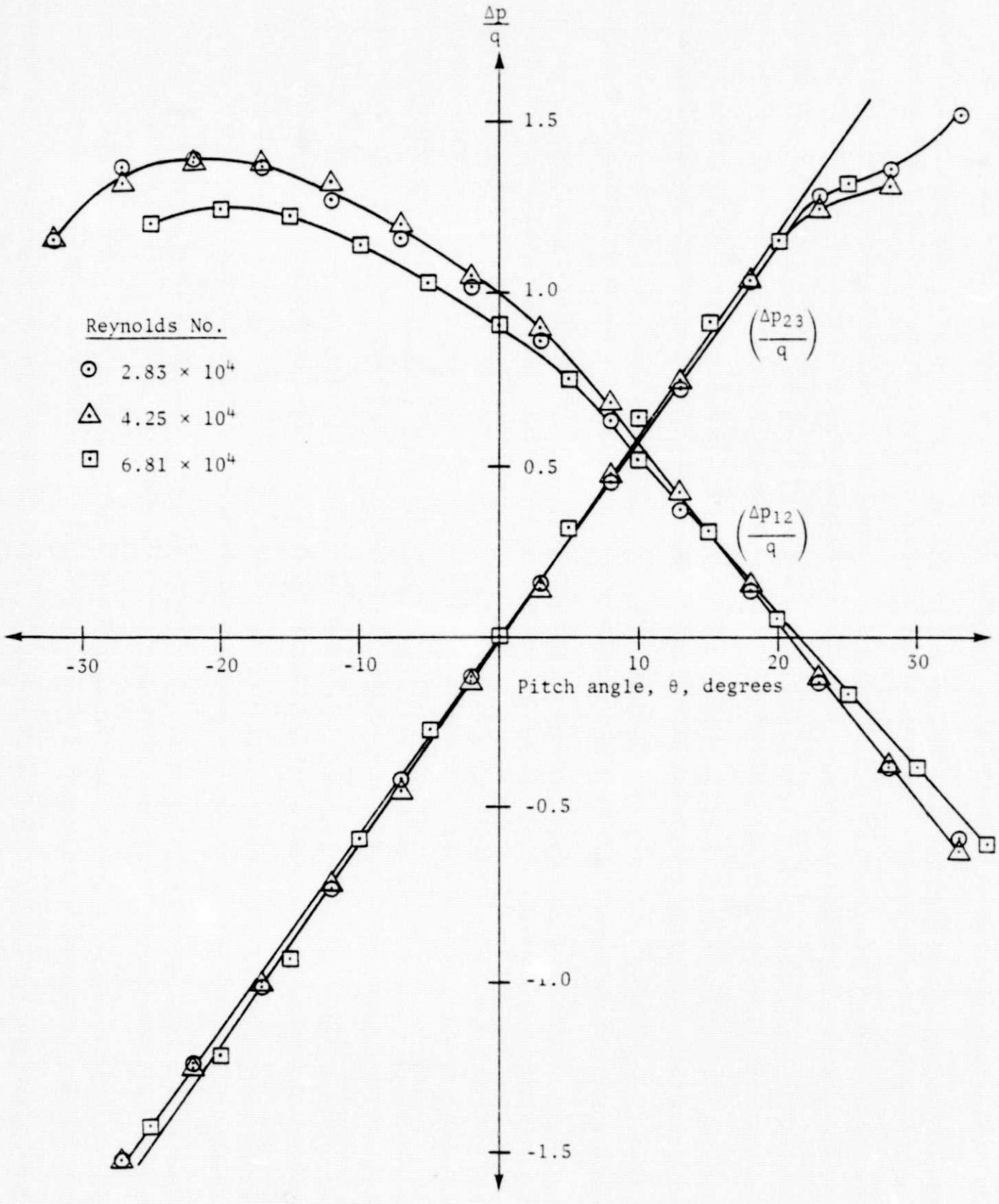

(a) Variation of nondimensional probe output $\Delta p/q$ with pitch angle in the range of +30 to -30 degrees

Figure 4. Probe calibration under steady flow conditions, ODU probe #2.

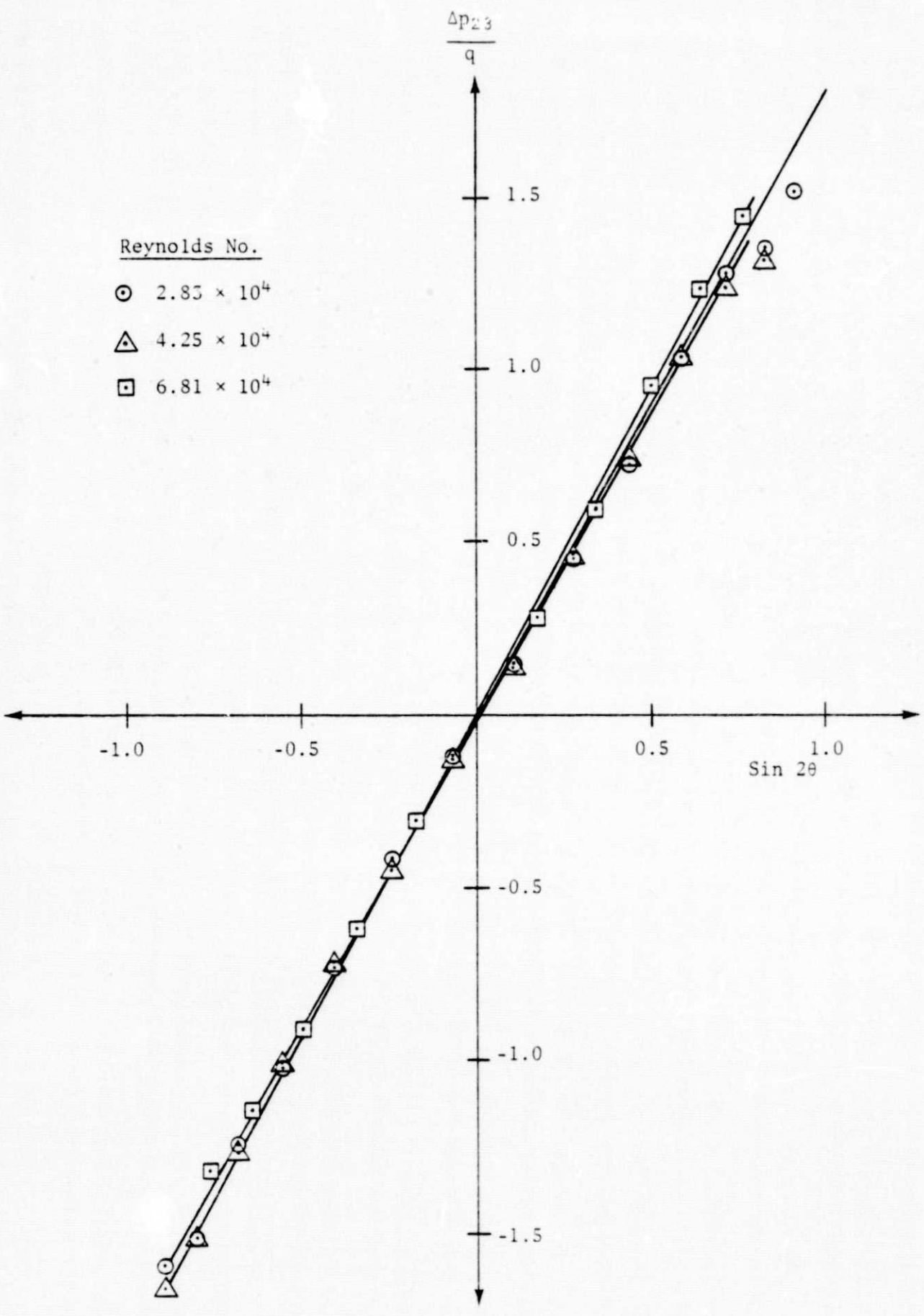

(b) $\Delta p_{23}/q$ against sin 2θ.

Figure 4. Continued.

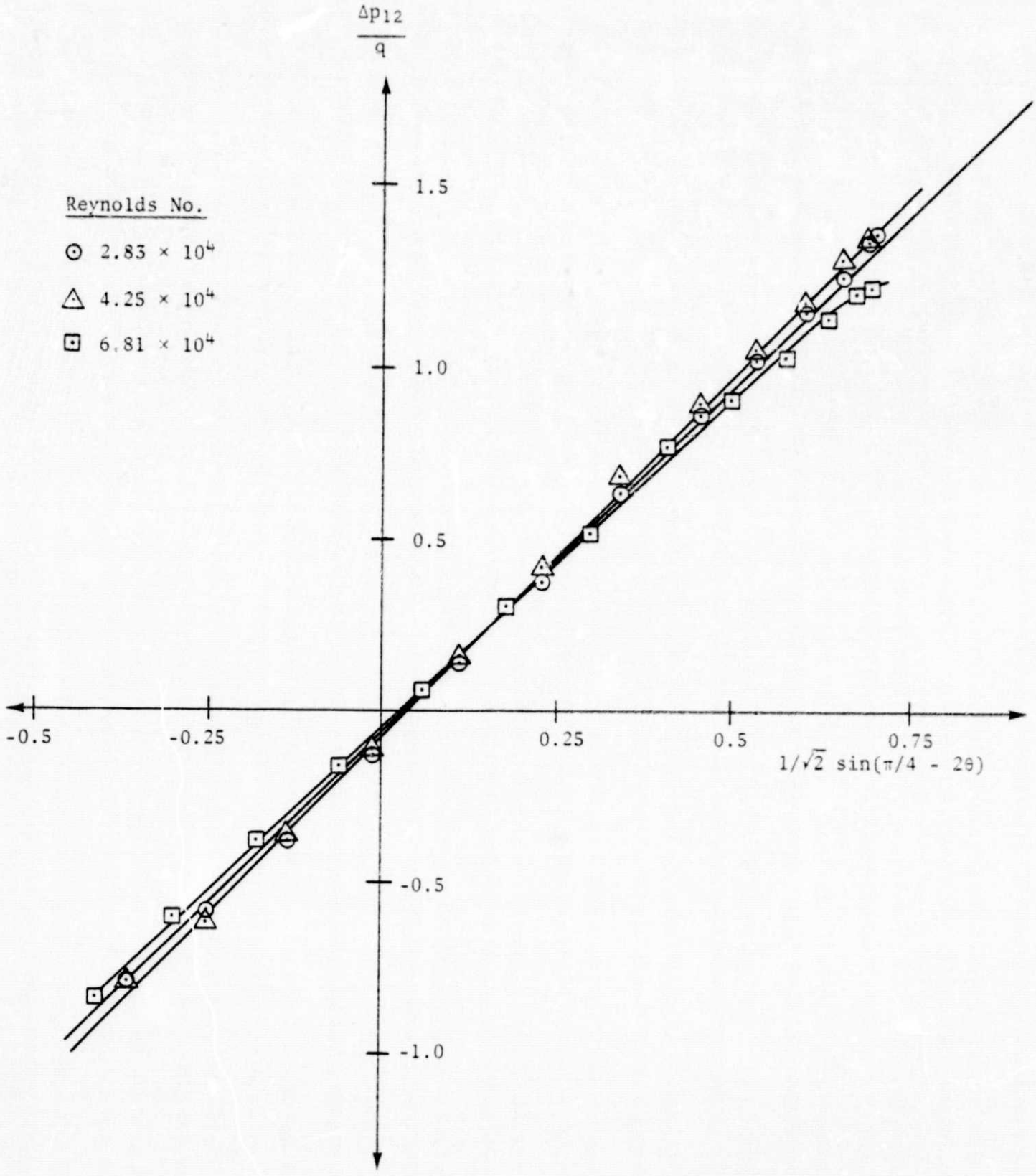

(c) $\Delta p_{12}/q$ against $1/\sqrt{2}\ \sin(\pi/4 - 2\theta)$

Figure 4. Continued.

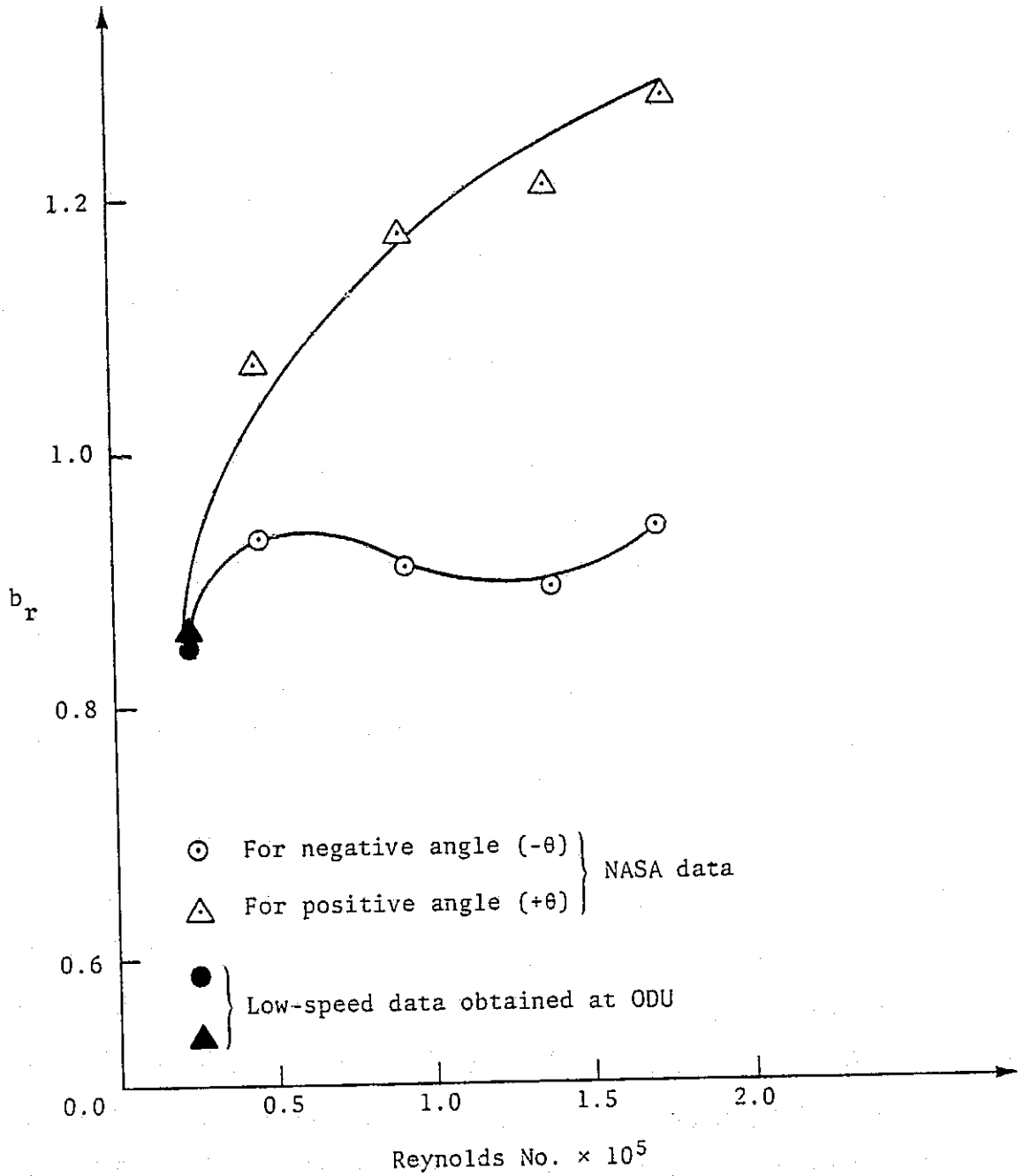

(d) Variation of ratio b_r with Reynolds number

Figure 4. Concluded

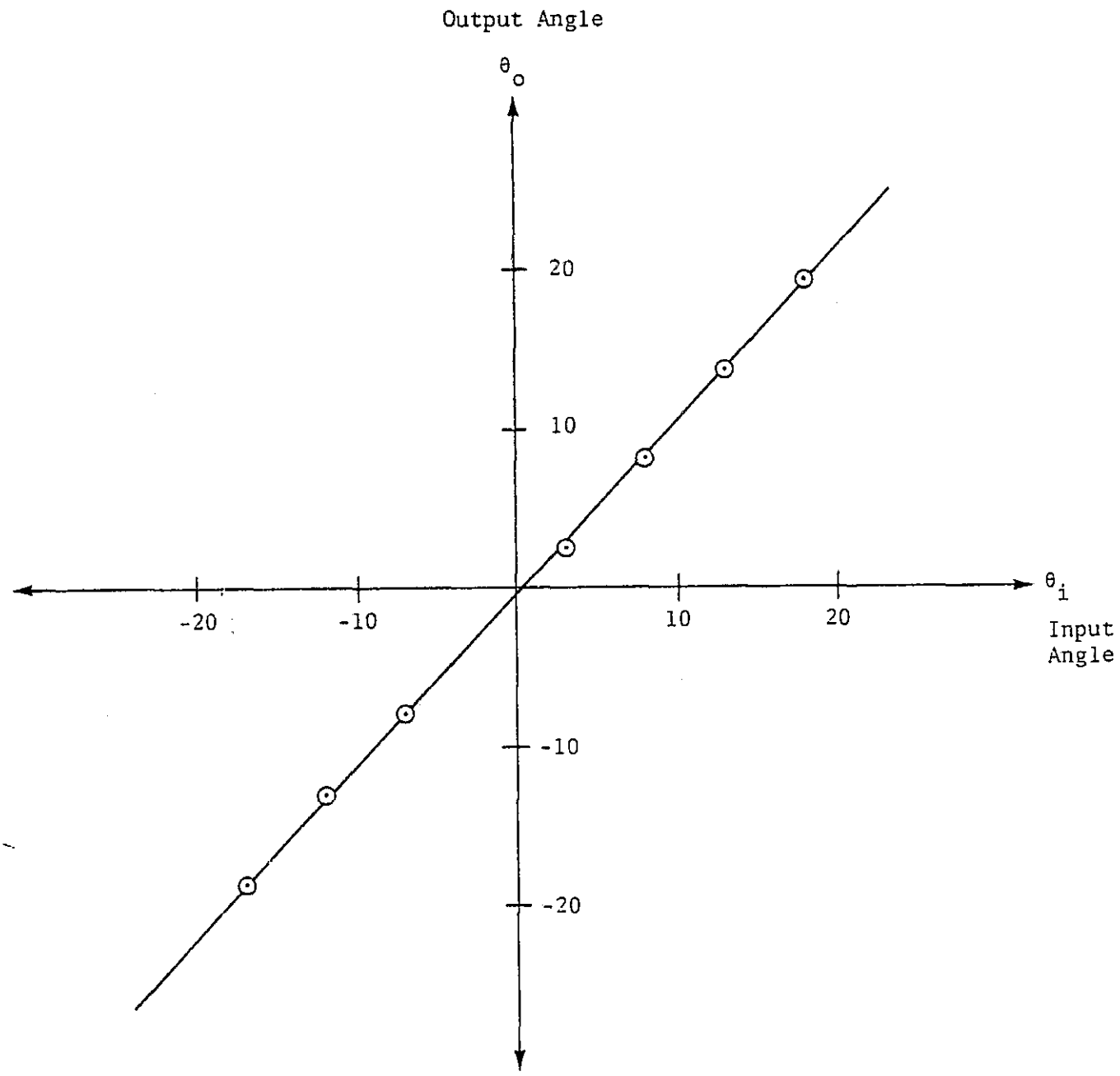

Figure 5. Variation of output angle θ_o with input angle θ_i under steady flow conditions for ODU probe #2. Output angle was calculated from pressure measurements with the aid of equation (8).

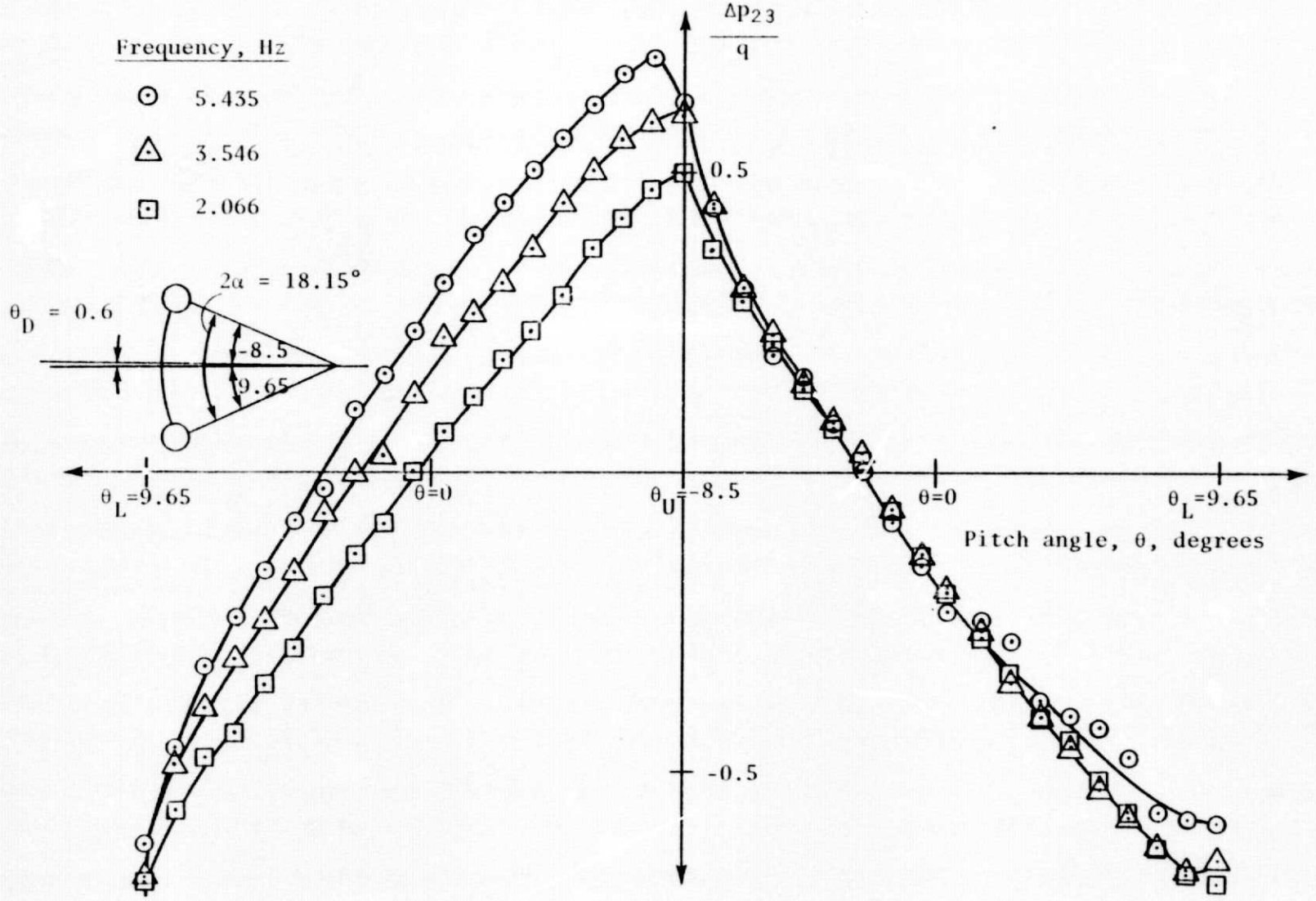

(a) $\Delta p_{23}/q$ at Reynolds no. 3.04×10^4

Figure 6. Probe characteristics under oscillating conditions for various frequencies when displacement angle θ_D = 0.6 degrees.

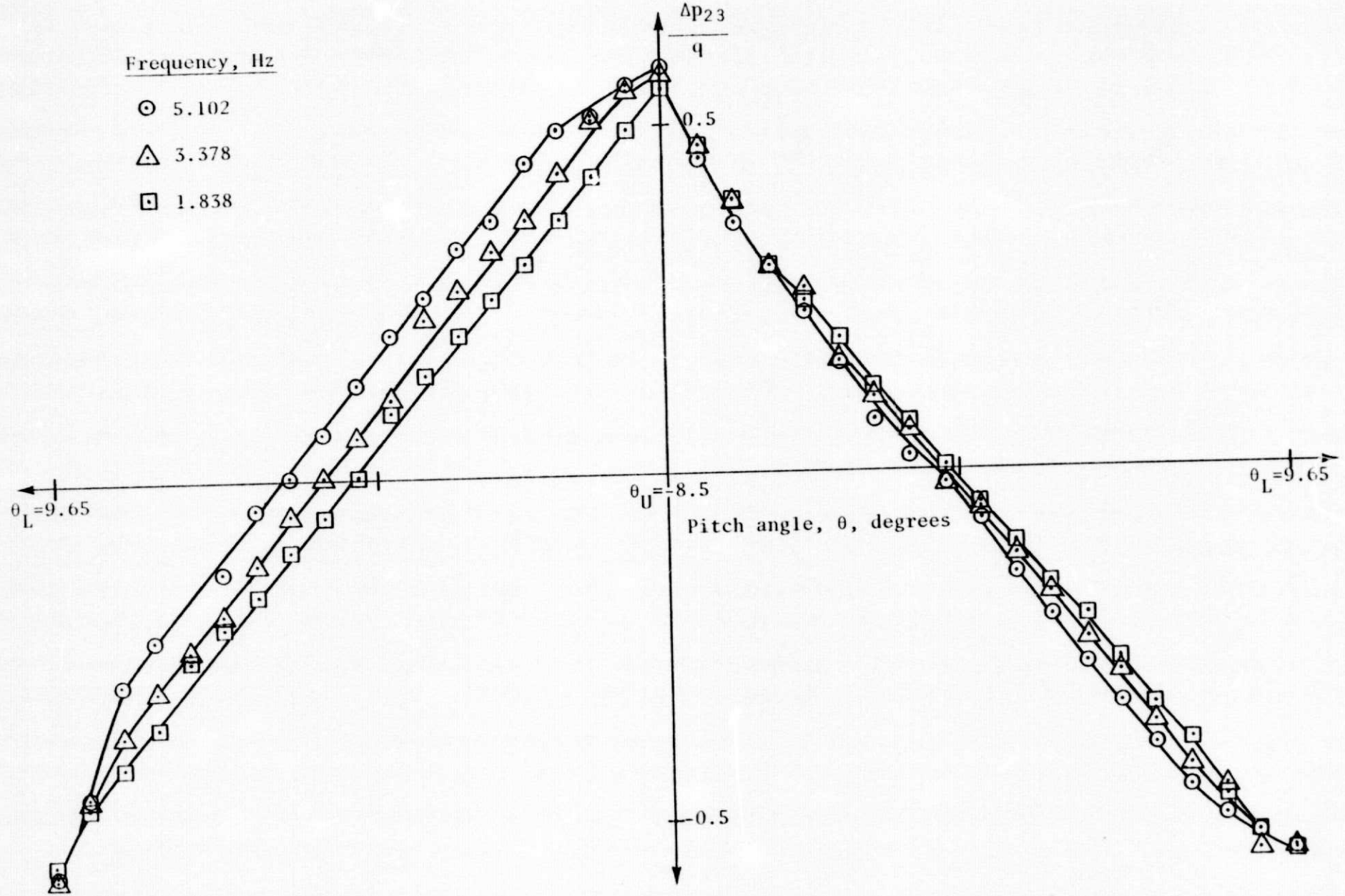

(b) $\Delta p_{23}/q$ at Reynolds no. 6.25×10^4

Figure 6. Continued.

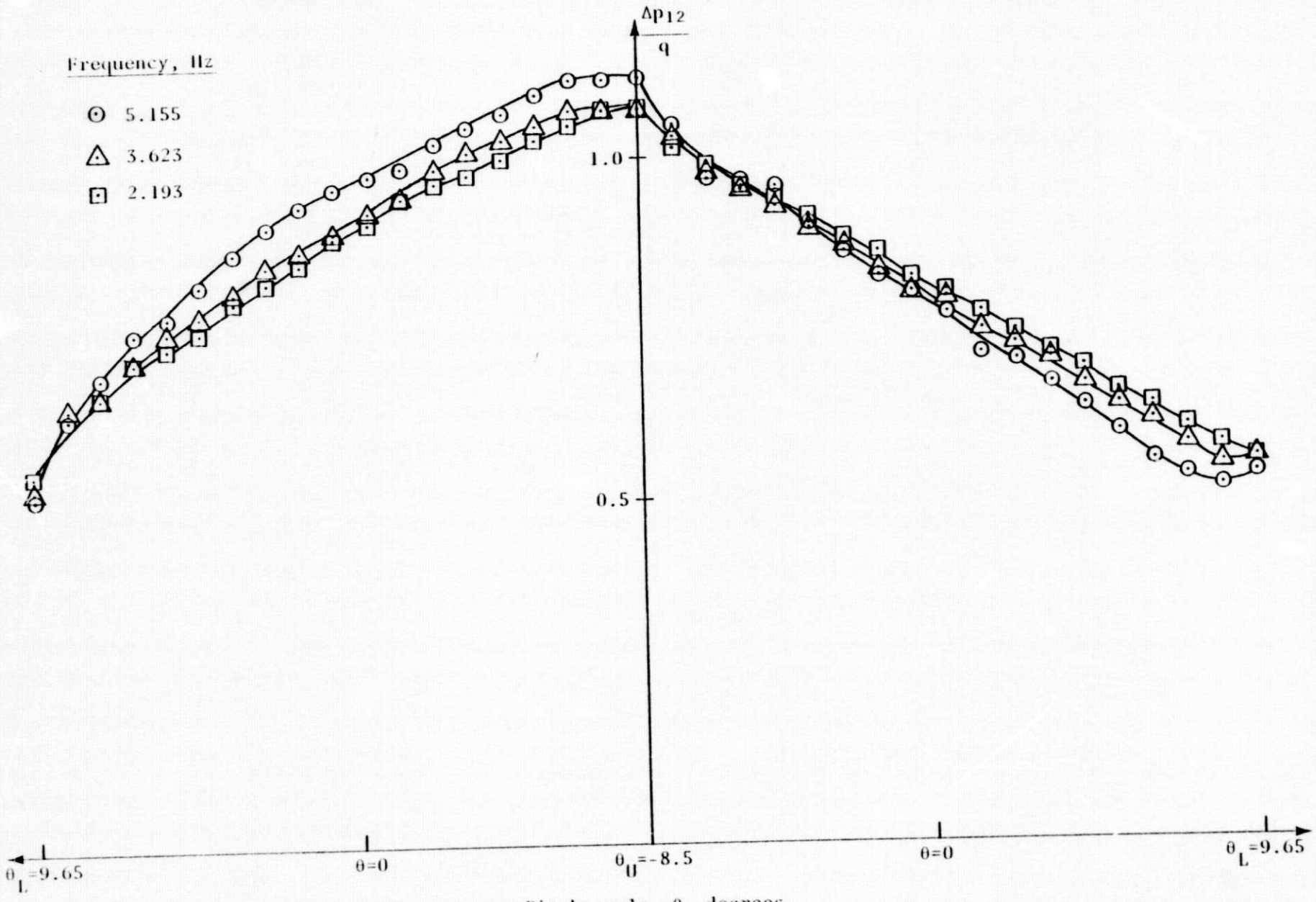

(c) $\Delta p_{12}/q$ at Reynolds No. 3.0×10^4

Figure 6. Continued

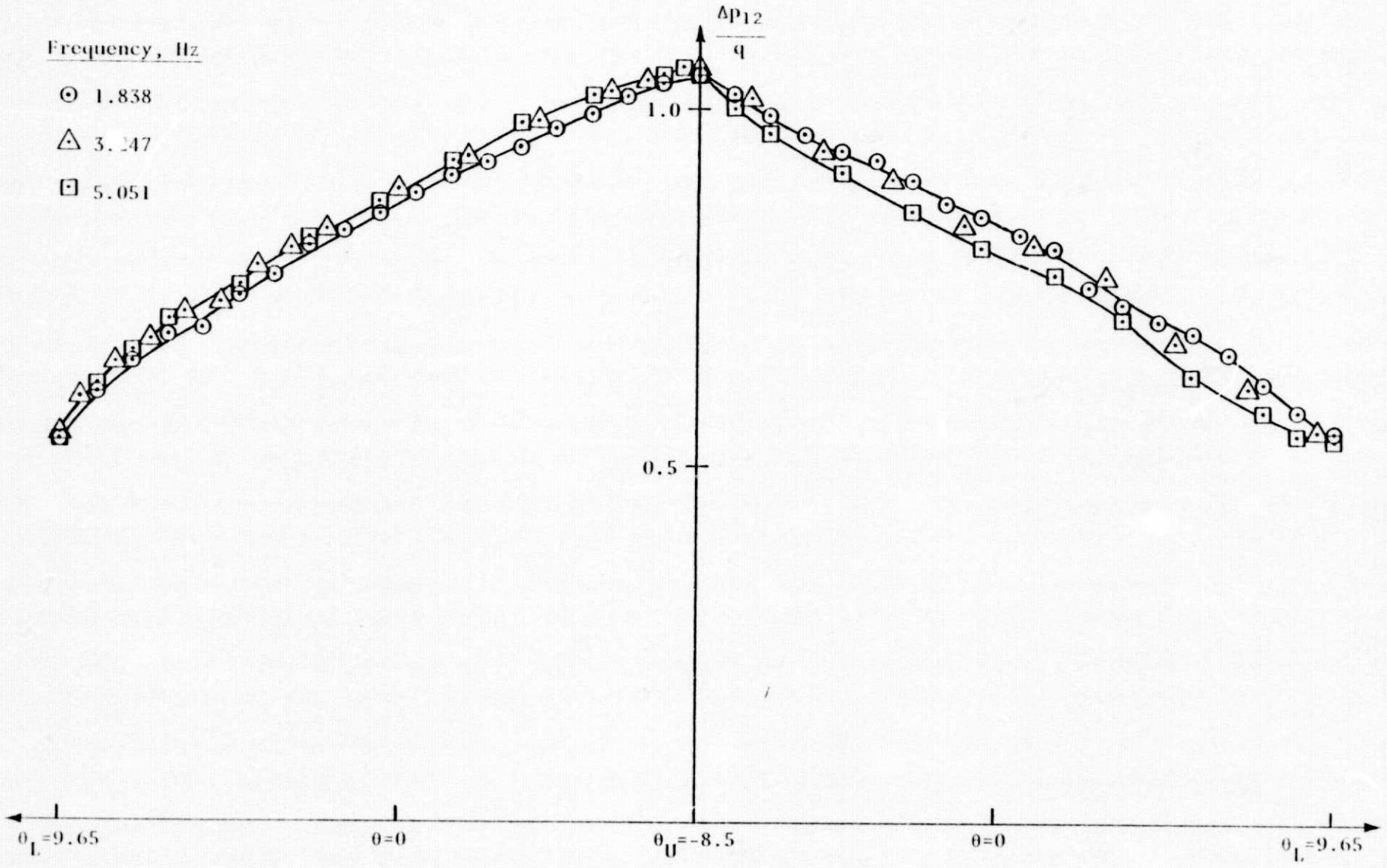

(d) $\Delta p_{12}/q$ at Reynolds No. 6.25×10^4

Figure 6. Concluded.

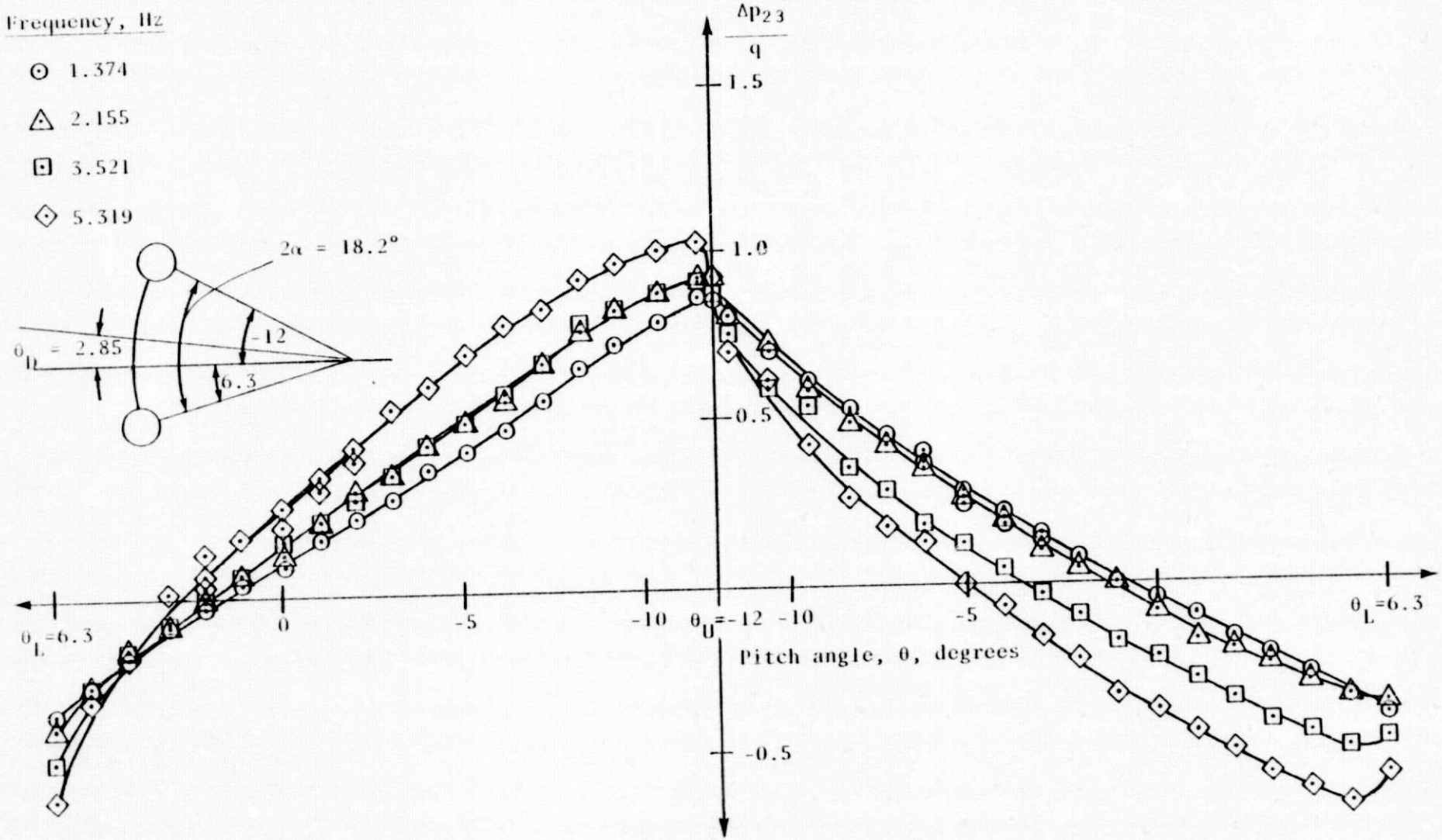

(a) $\Delta p_{23}/q$ at Reynolds No. 2.38×10^4

Figure 7. Probe characteristics under oscillating conditions for various frequencies when displacement angle θ_D = 2.85 degrees.

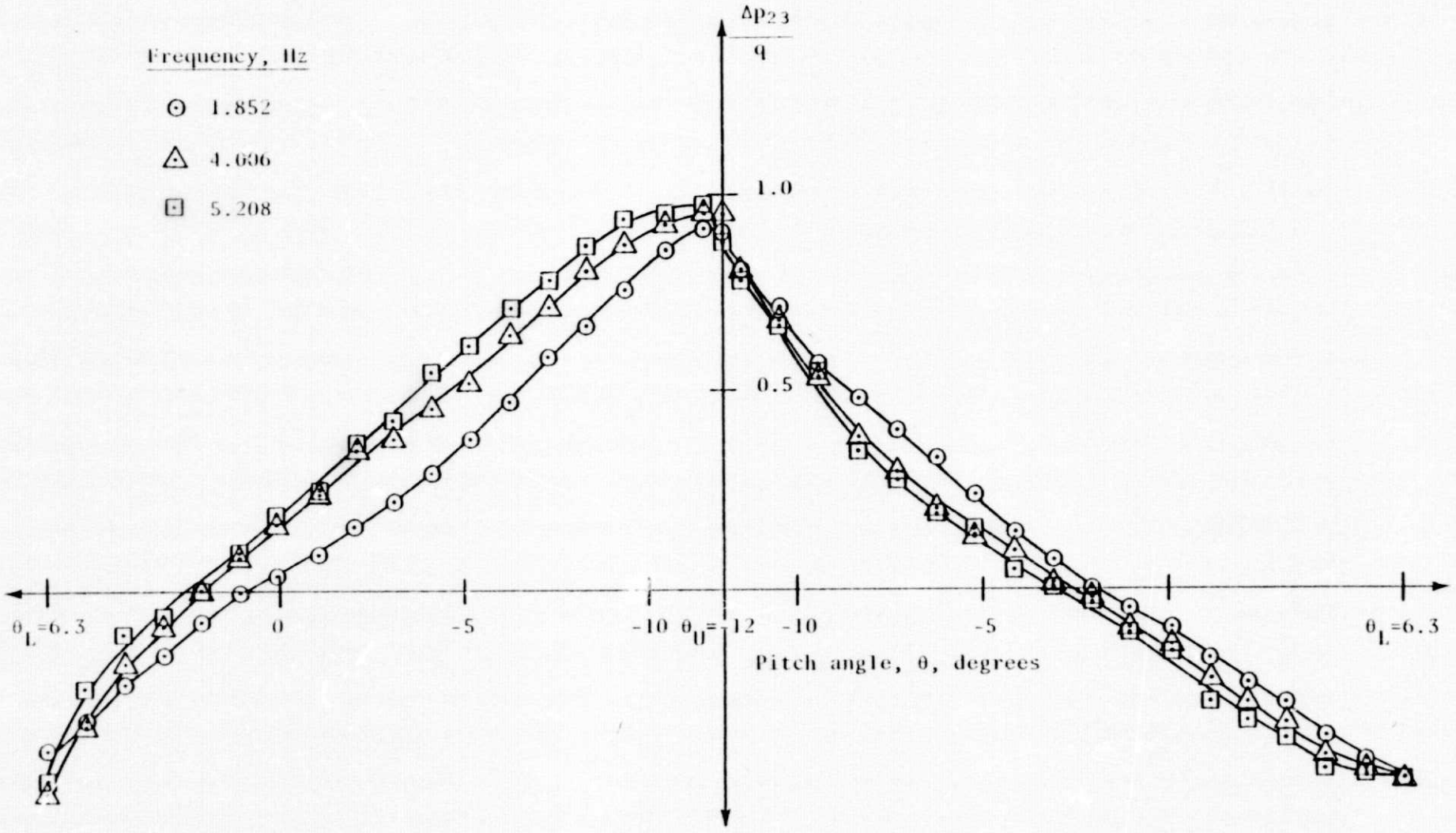

(b) $\Delta p_{23}/q$ at Reynolds No. 3.58×10^4

Figure 7. Continued.

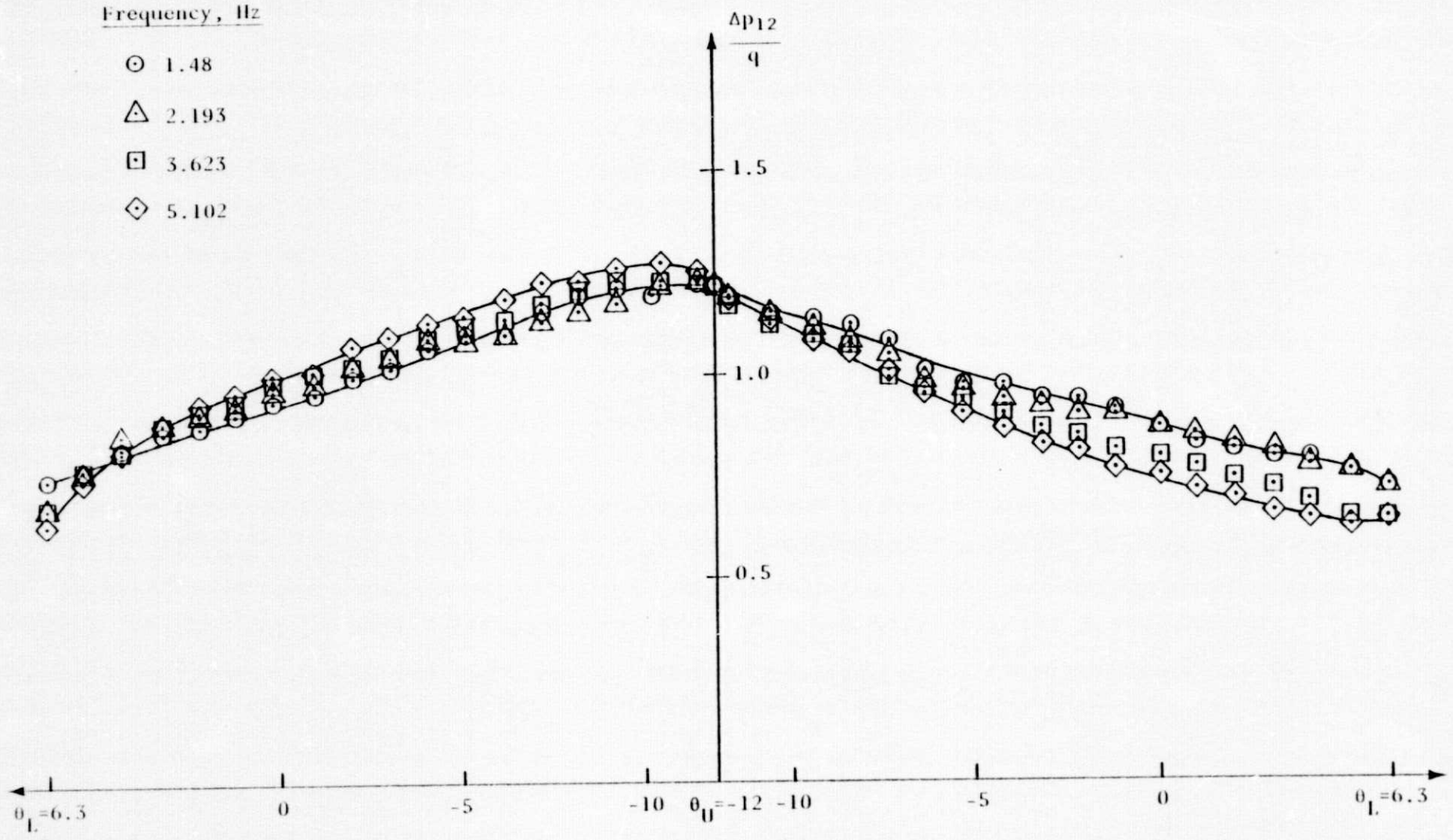

(c) $\Delta p_{12}/q$ at Reynolds No. 2.38×10^4

Figure 7. Continued.

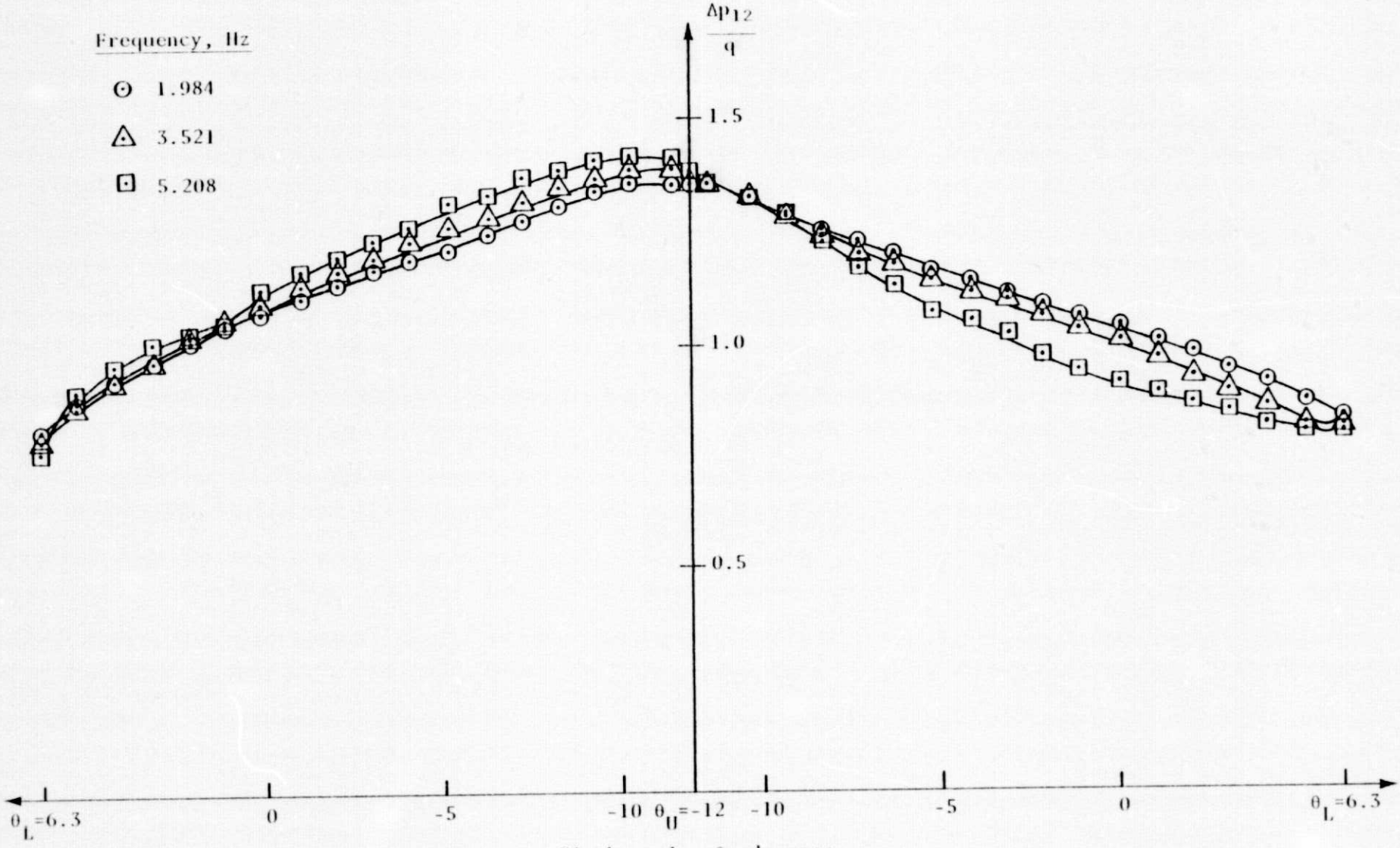

(d) $\Delta p_{12}/q$ at Reynolds No. 3.58×10^4

Figure 7. Concluded.

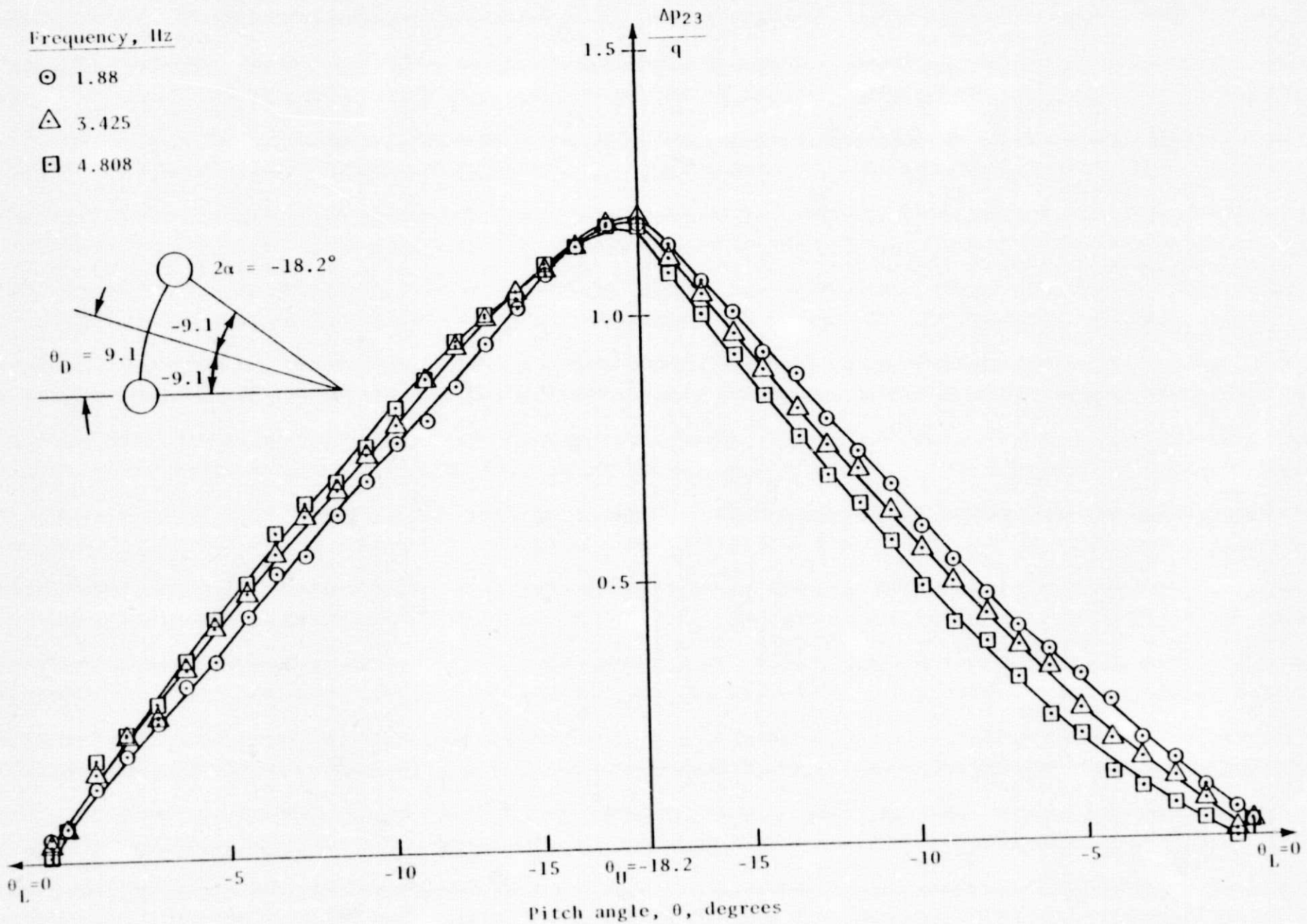

(a) $\Delta p_{23}/q$ at Reynolds No. 6.25×10^4

Figure 8. Probe characteristics under oscillating conditions for various frequencies when displacement angle θ_D = 9.1 degrees.

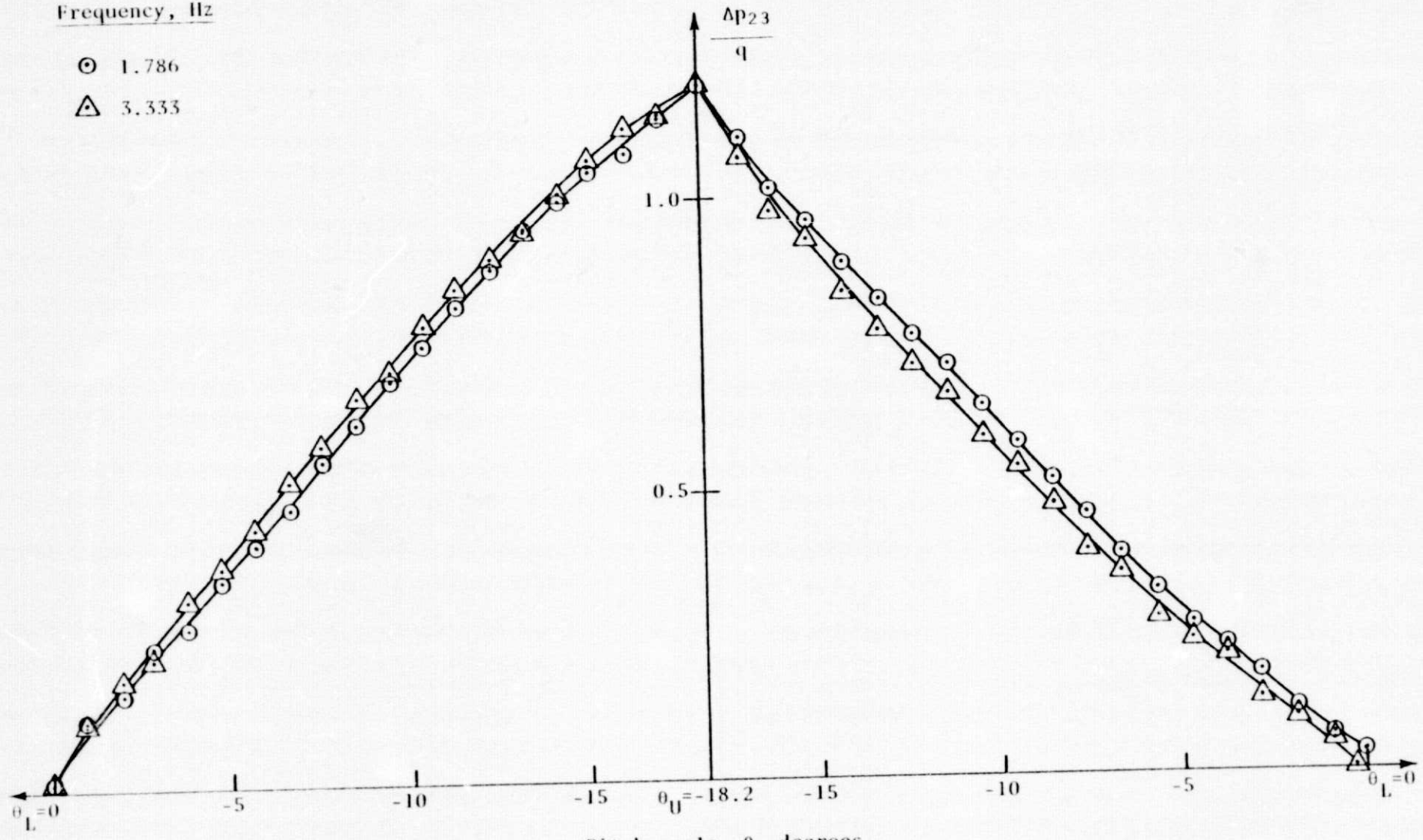

(b) $\Delta p_{23}/q$ at Reynolds No. 6.25×10^4

Figure 8. Continued.

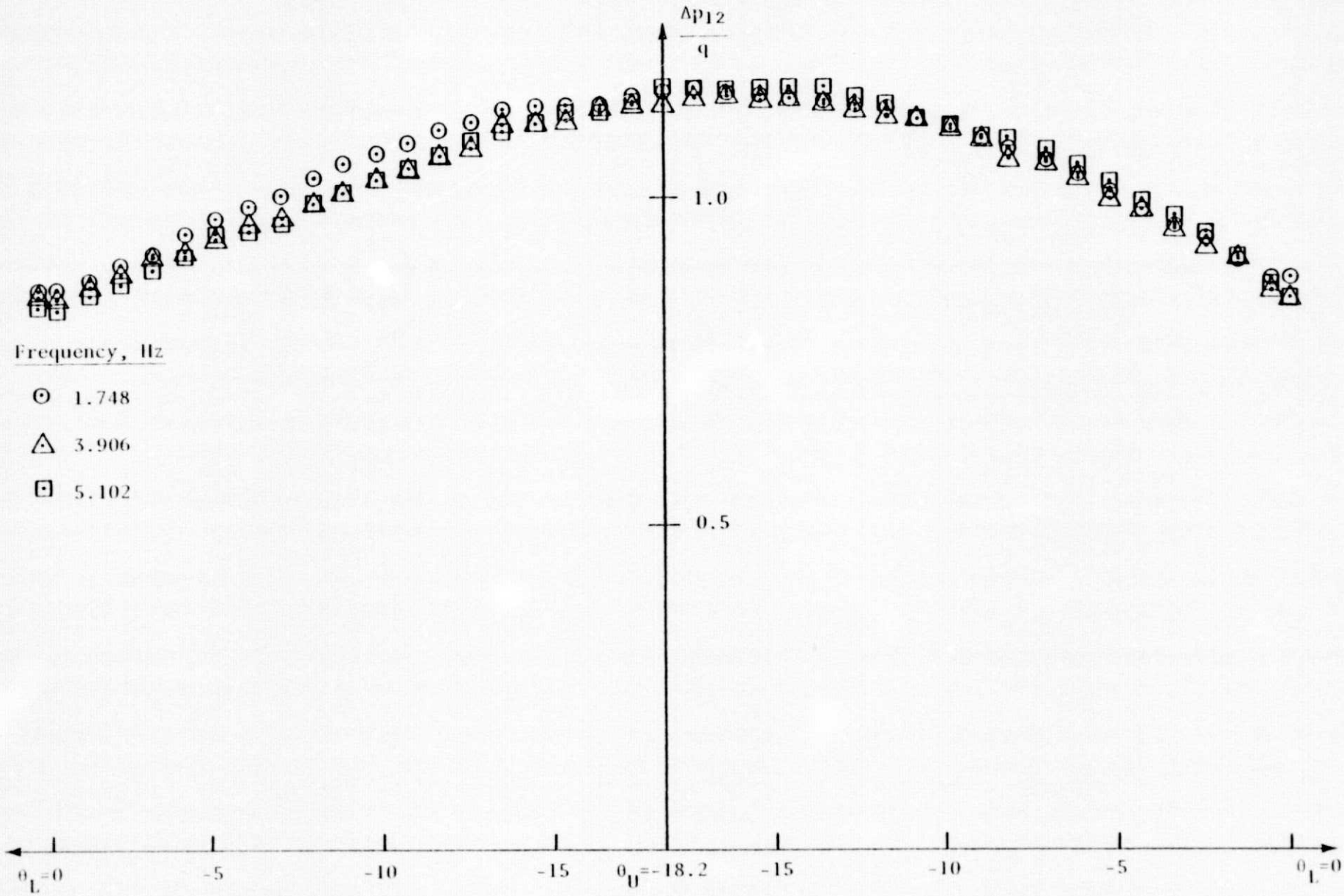

(c) $\Delta p_{12}/q$ at Reynolds No. 6.25×10^4

Figure 8. Concluded.

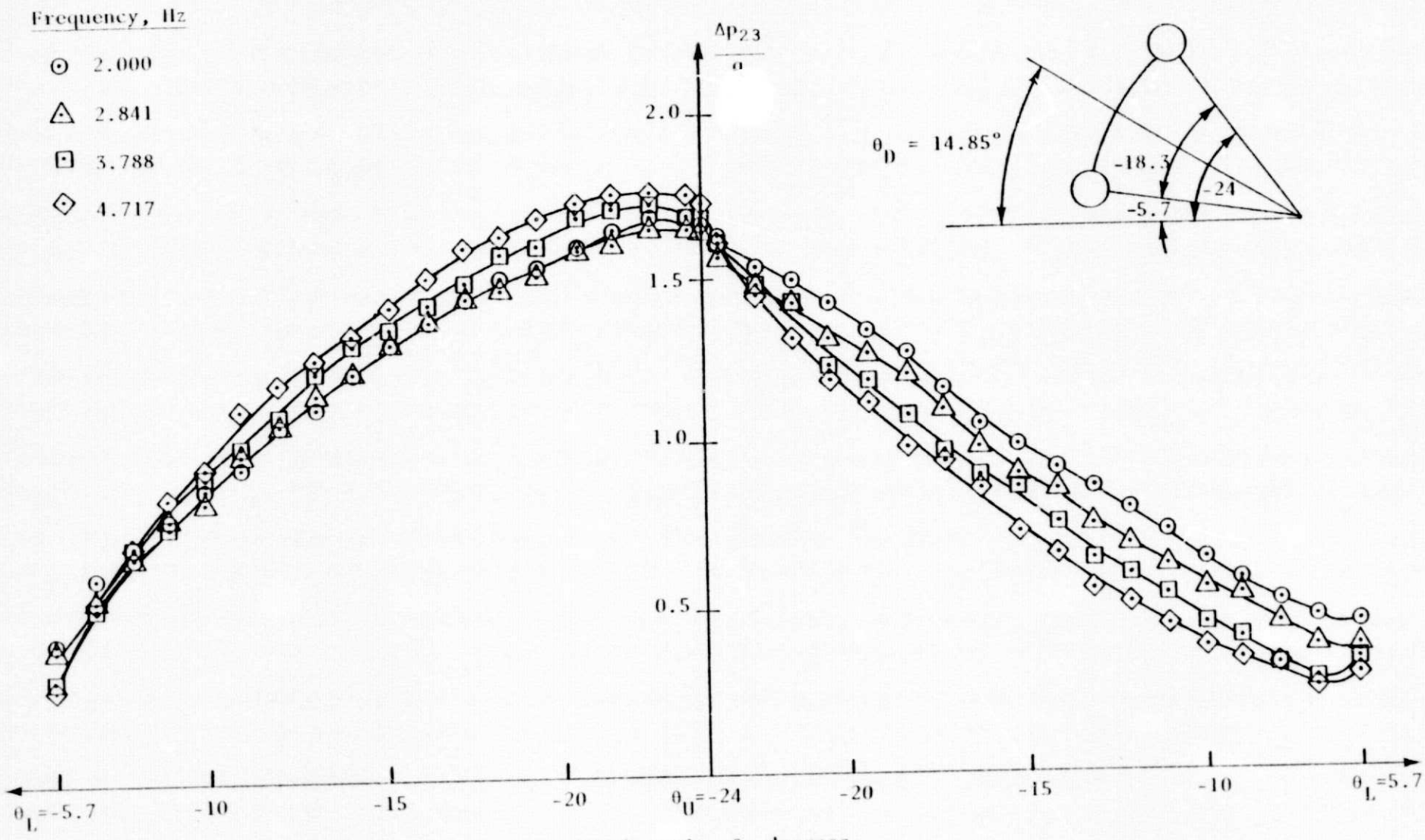

(a) $\Delta p_{23}/q$ at Reynolds No. 2.38×10^4

Figure 9. Probe characteristics under oscillating conditions for various frequencies when displacement angle θ_D = 14.85 degrees.

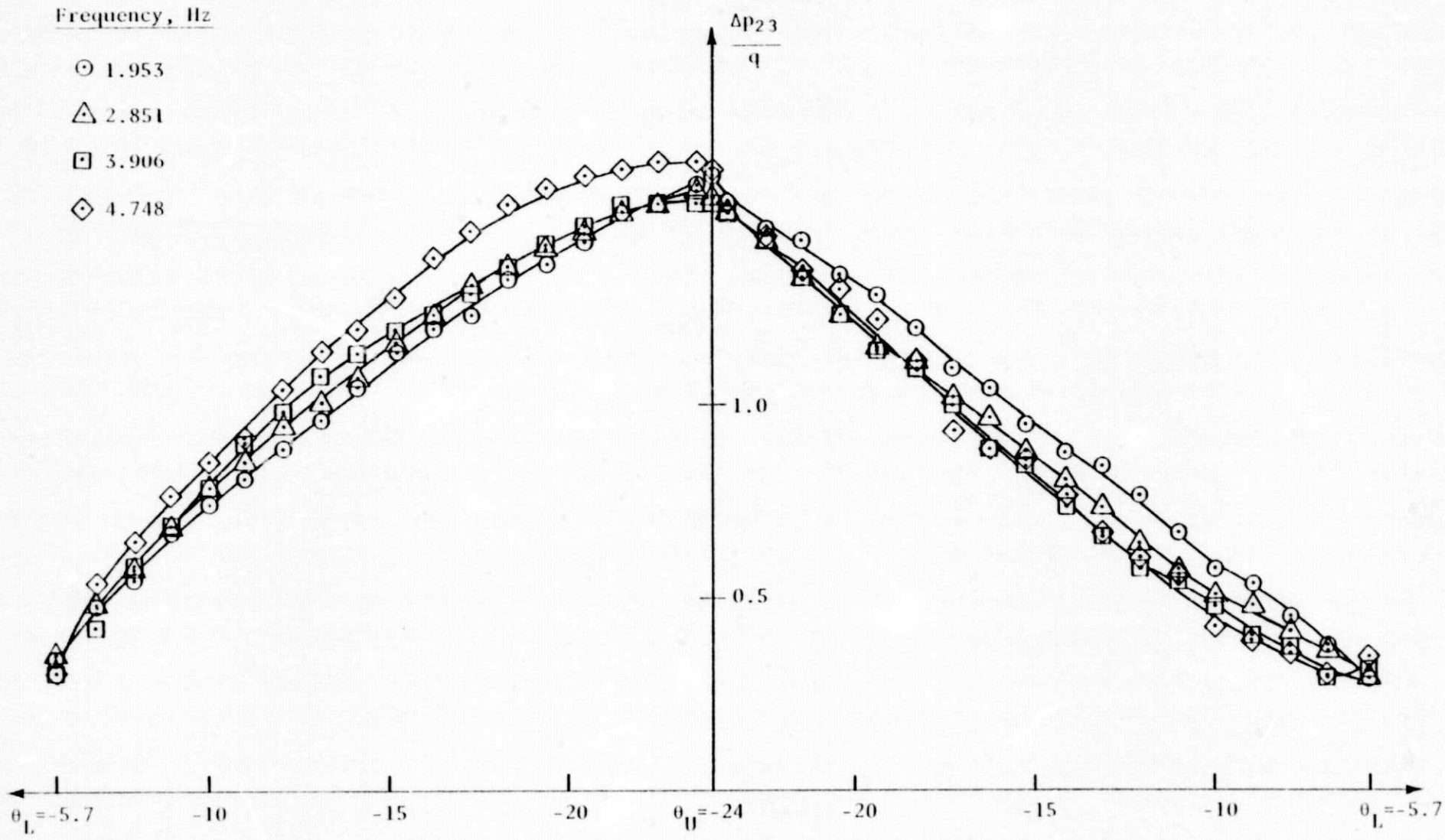

(b) $\Delta p_{23}/q$ at Reynolds No. 3.58×10^4

Figure 9. Continued.

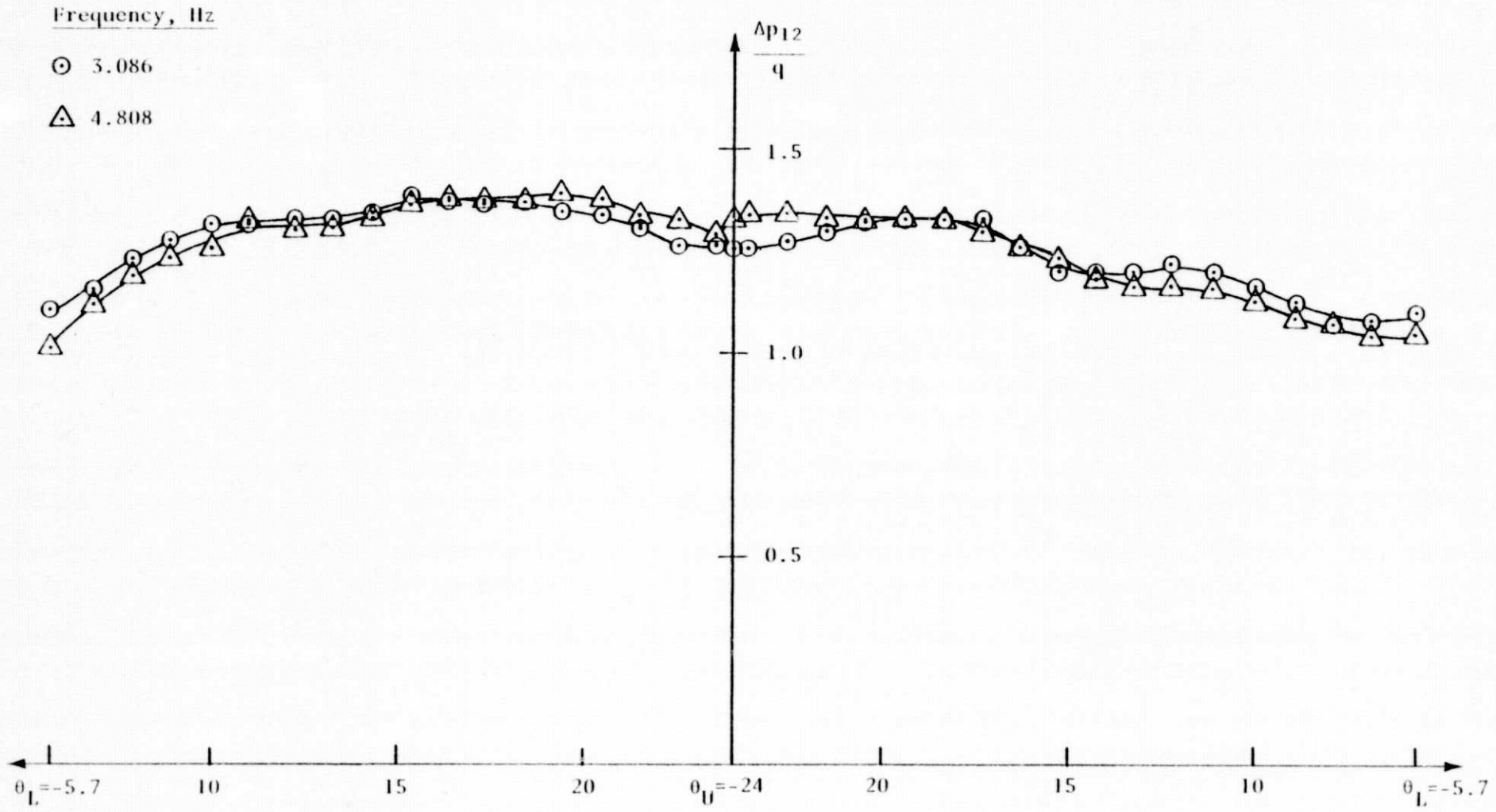

(c) $\Delta p_{12}/q$ at Reynolds No. 2.38×10^4

Figure 9. Continued.

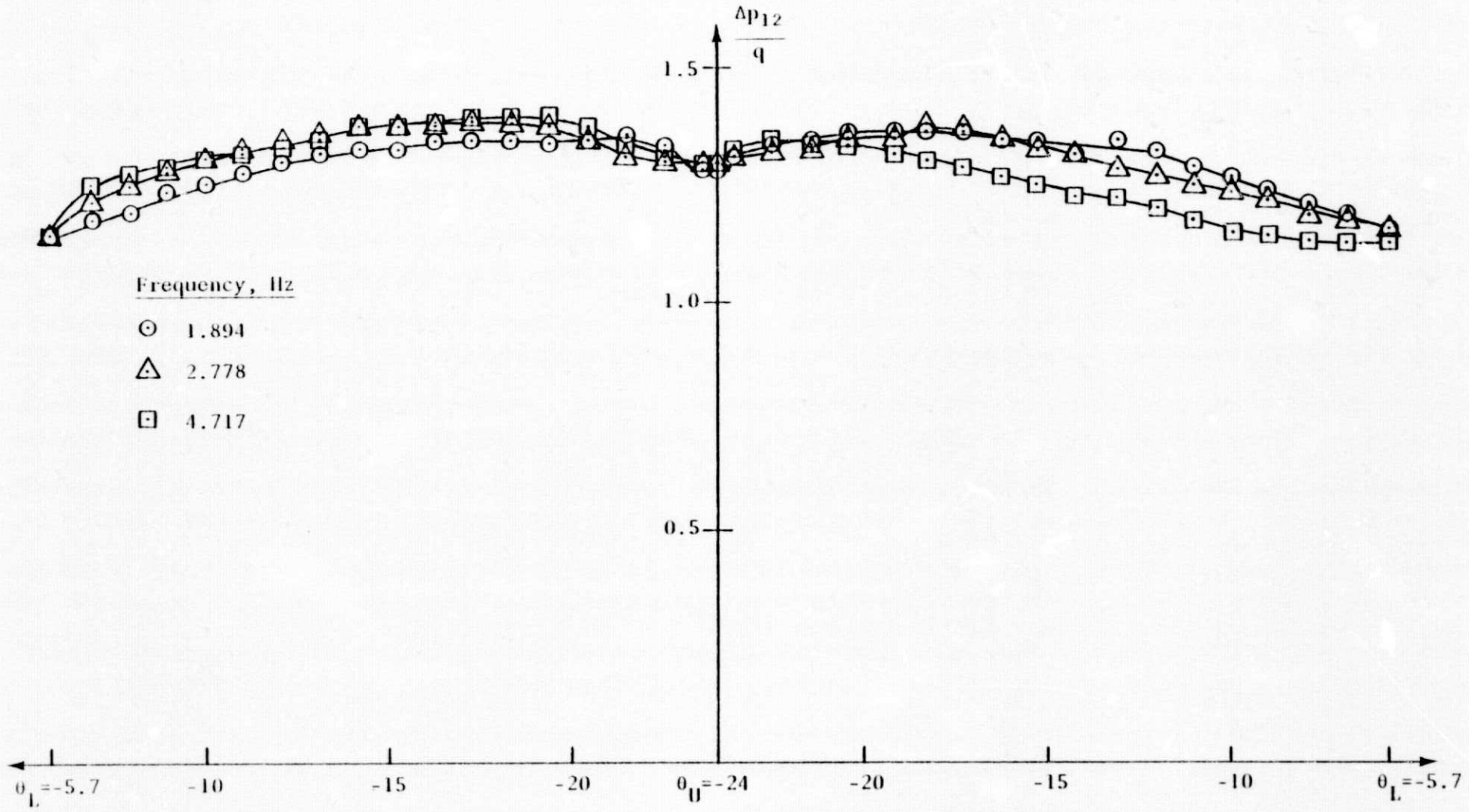

(d) $\Delta p_{12}/q$ at Reynolds No. 3.58×10^4

Figure 9. Concluded.

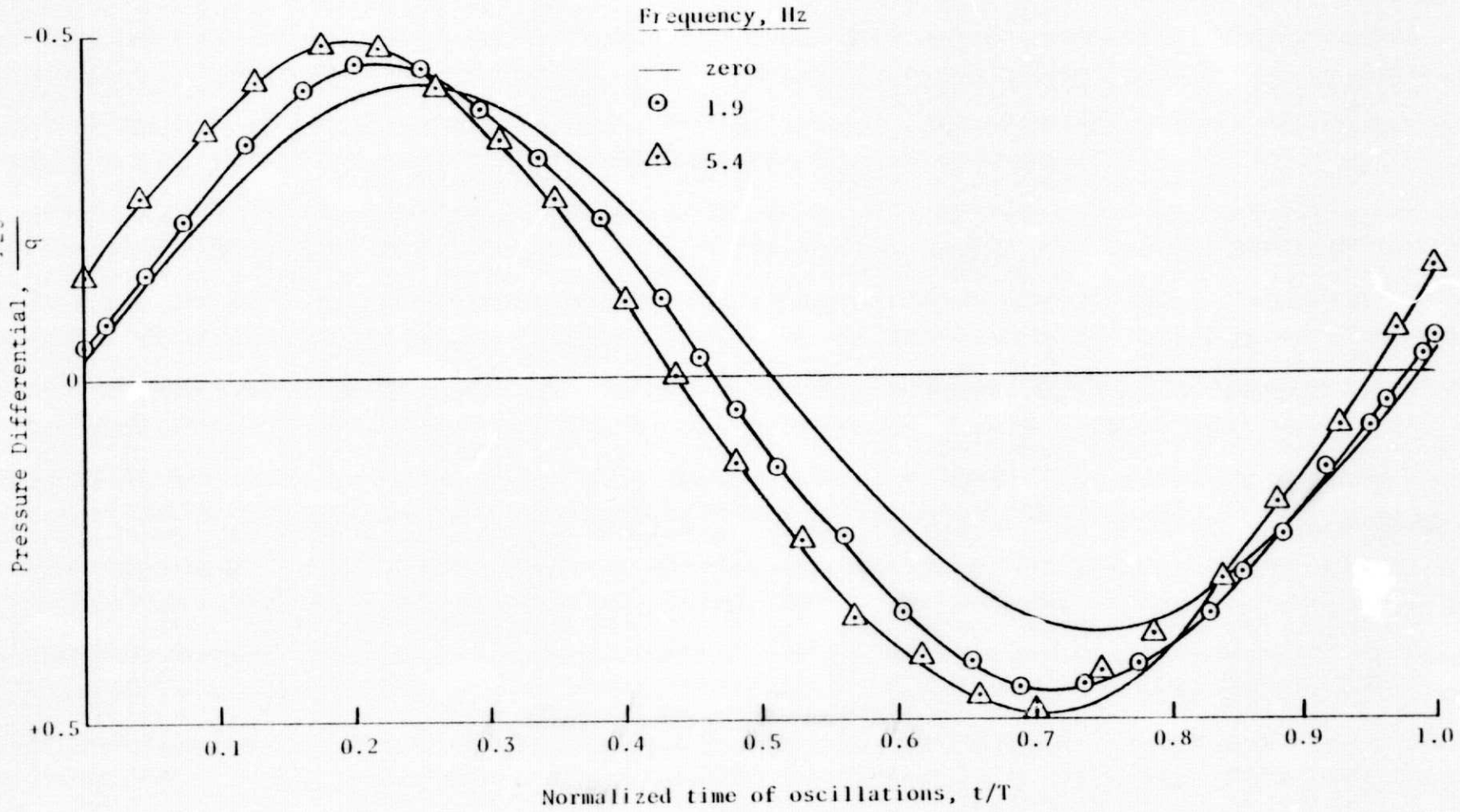

(a) Variation of $\Delta p_{23}/q$

Figure 10. Variation of pressure differential with frequency during a period T for constant Reynolds number, Re = 6.25×10^4.

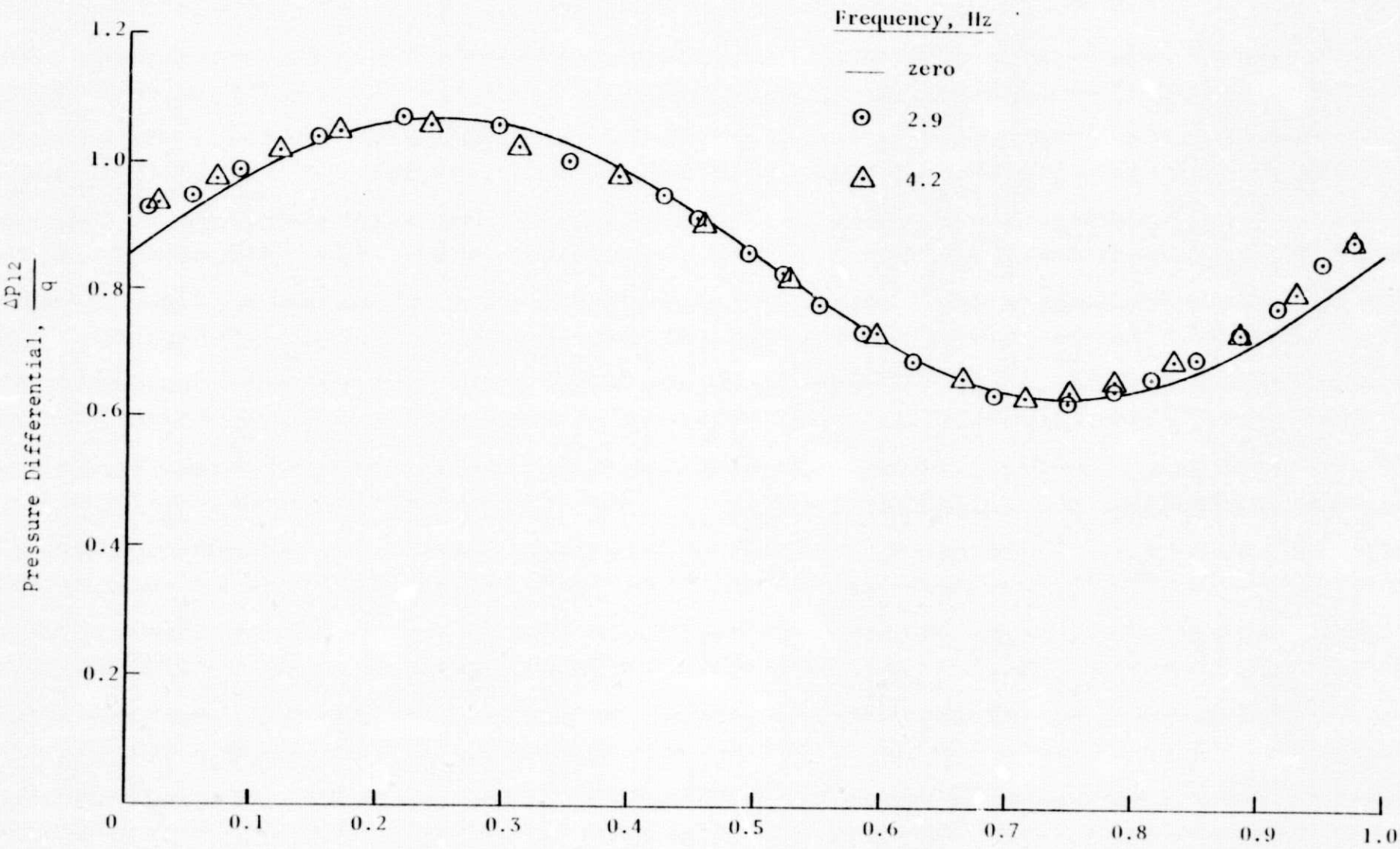

(b) Variation of $\Delta p_{12}/q$

Figure 10. Continued.

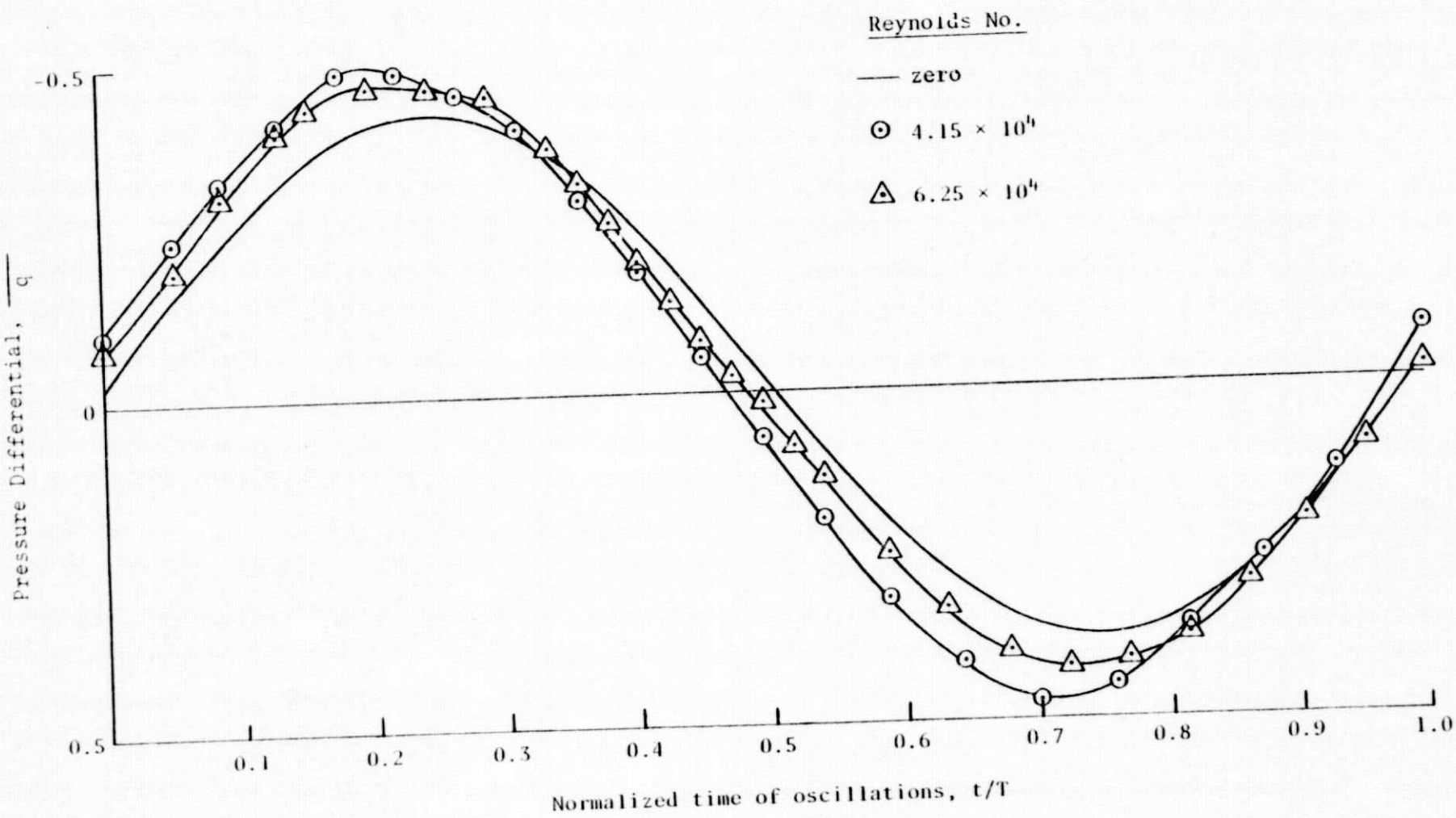

(a) Variation of $\Delta p_{23}/q$

Figure 11 Variation of pressure differential with Reynolds number for constant frequency, f = 2.9 Hz.

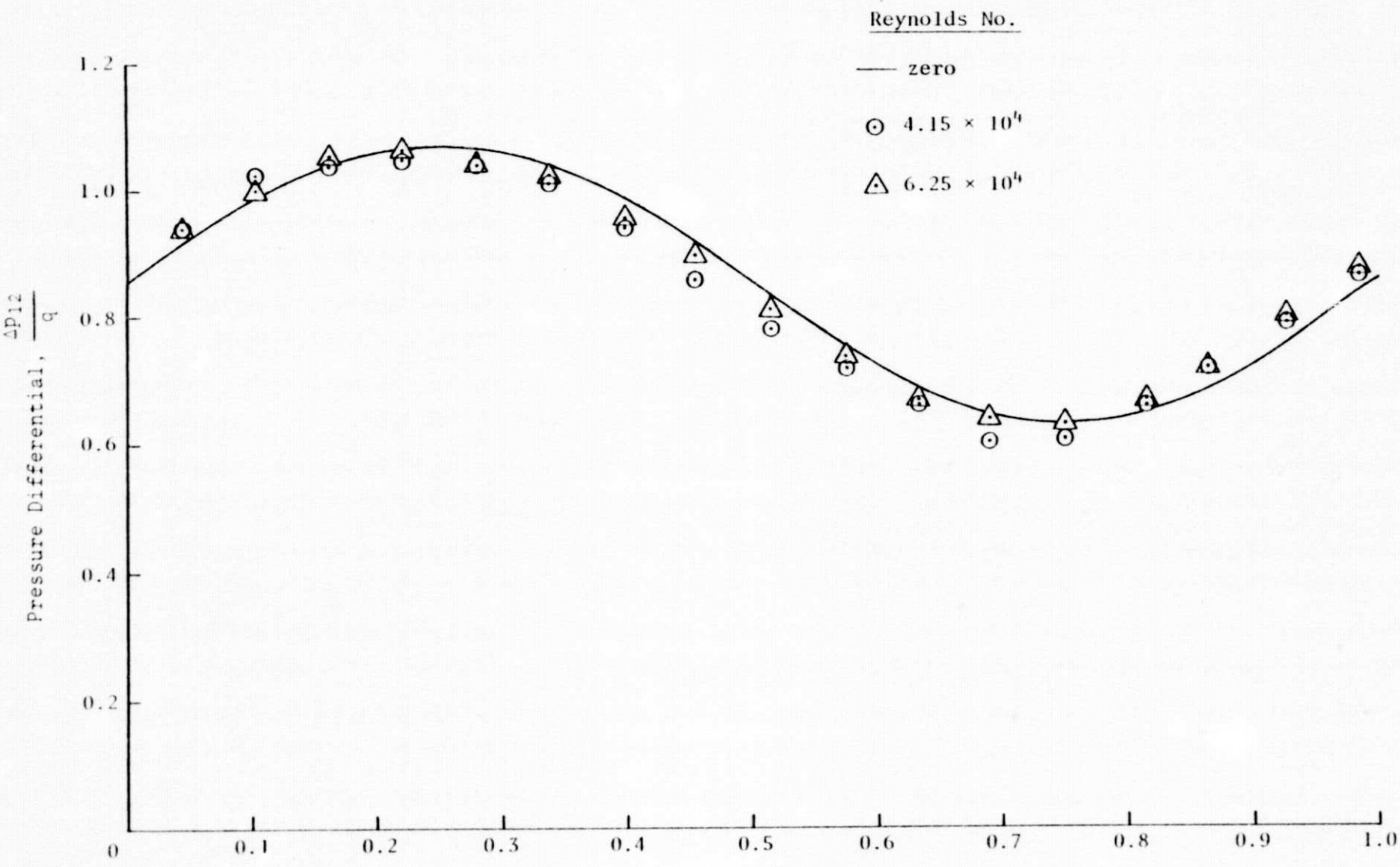

(b) Variation of $\Delta p_{12}/q$

Figure 11. Concluded.

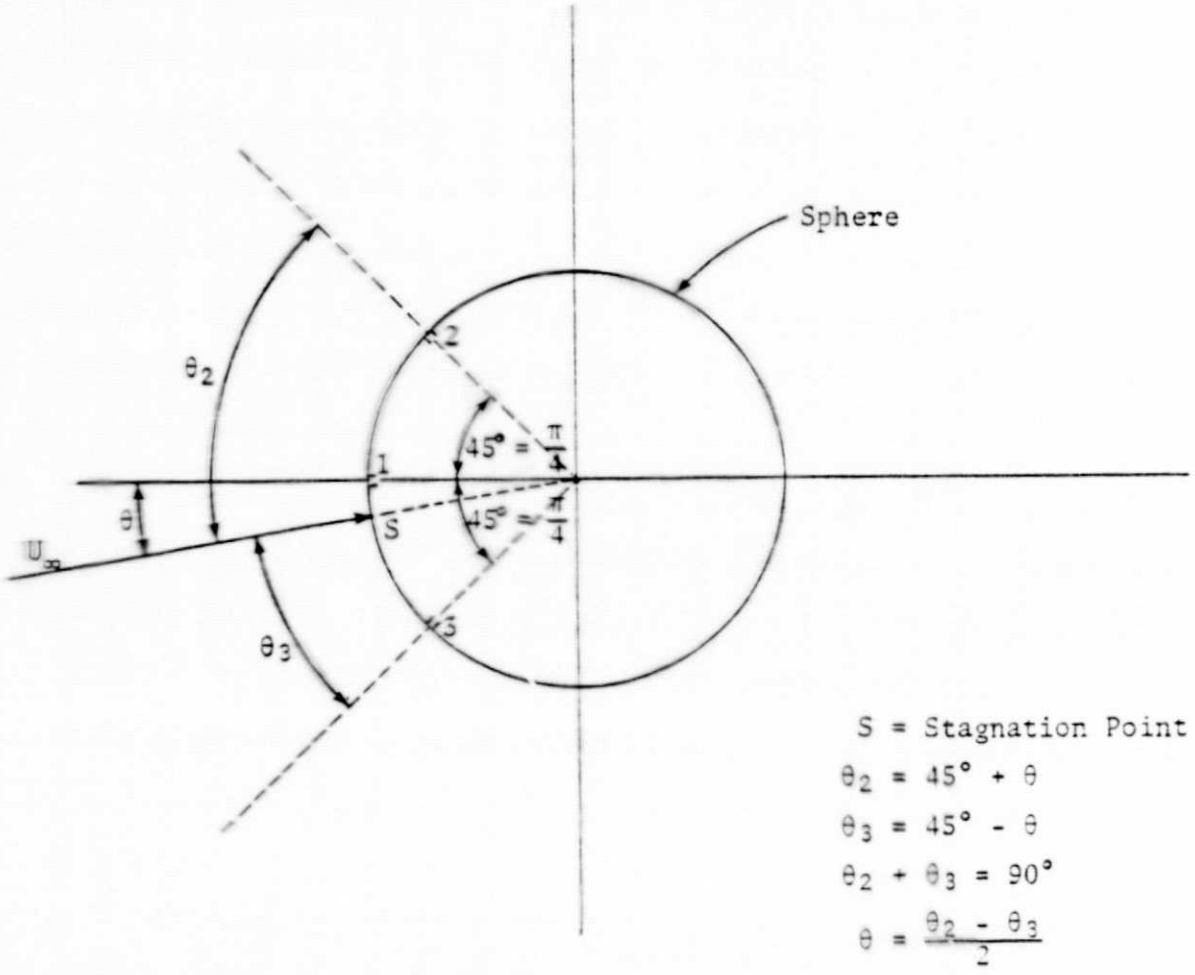

Figure A1. Flow around a sphere.